HHS Public Access

Author manuscript

J Proteome Res. Author manuscript; available in PMC 2023 May 02.

Published in final edited form as:

J Proteome Res. 2021 October 01; 20(10): 4815–4830. doi:10.1021/acs.jproteome.1c00500.

Integrated Phosphoproteomics for Identifying Substrates of Human Protein Kinase A *(PRKACA)* and Its Oncogenic Mutant *DNAJB1 - PRKACA*

Adak Karamafrooz,
Department of Biochemistry, Molecular Biology, and Biophysics, University of Minnesota, Minneapolis, Minnesota 55455, United States

Jack Brennan,
Independent Technology Consultant, LIC, Boston, Massachusetts 02129, United States

David D. Thomas,
Department of Biochemistry, Molecular Biology, and Biophysics, University of Minnesota, Minneapolis, Minnesota 55455, United States

Laurie L. Parker
Department of Biochemistry, Molecular Biology, and Biophysics, University of Minnesota, Minneapolis, Minnesota 55455, United States

Abstract

The *DNAJB1-PRKACA* fusion is the signature genetic event of fibrolamellar hepatocellular carcinoma (FL-HCC), a rare but lethal liver cancer that primarily affects adolescents and young adults. A deletion fuses the first exon of the HSP40 gene *(DNAJB1),* with exons 2–10 of protein kinase A *(PRKACA),* producing the chimeric kinase DNAJB1-PKA$_{ca}$ (J-PKA$_{ca}$). The HSP40 portion's scaffolding/chaperone function has been implicated in redirecting substrate recognition to upregulate oncogenic pathways, but the direct substrates of this fusion are not fully known. We integrated cell-based and *in vitro* phosphoproteomics to identify substrates targeted directly by PKA and J-PKA$_{ca}$, comparing phosphoproteome profiles from cells with *in vitro* rephosphorylation of peptides and proteins from lysates using recombinant enzymes. We identified a subset of phosphorylation sites in both cell-based and *in vitro* experiments, as well as altered

Corresponding Author Laurie L. Parker llparker@umn.edu.
Current affiliation: Department of Diabetes Complications and Metabolism, Beckman Research Institute, City of Hope, Duarte, California 91010, United States

ASSOCIATED CONTENT

Supporting Information

The Supporting Information is available free of charge at https://pubs.acs.org/doi/10.1021/acs.jproteome.1c00500.
SDS-PAGE gel showing recombinant PKA$_{ca}$ and J-PKA$_{ca}$ expression and purification (Figure S1); kinase activity assay confirming active recombinant PKA$_{ca}$ and J-PKA$_{ca}$ (Figure S2); Western blot confirming PKA$_{ca}$ and J-PKA$_{ca}$ in HEK293 cells (Figure S3) (PDF)
Outputs from PEAKS results processed through the PEAKS-ModExtractor script; compare all with tumor > normal summary.xlsx (Table S1); list of PKA direct sites from Sugiyama Scientific Repts 2019.xlsx (Table S2); IPA comparison table, Turnham, J-PKAca–WT PKA.xlsx (Table S3); IPA comparison table inhibitor-persistent sites.xlsx (Table S4) (ZIP)

Complete contact information is available at: https://pubs.acs.org/10.1021/acs.jproteome.1c00500

The authors declare no competing financial interest.

pathways and proteins consistent with observations from related studies. We also treated cells with PKA inhibitors that function by two different mechanisms (rpcAMPs and PKI) and examined phosphoproteome profiles, finding some substrates that persisted in the presence of inhibitors and revealing differences between WT and chimera. Overall, these results provide potential insights into J-PKA$_{ca}$'s oncogenic activity in a complex cellular system and may provide candidate targets for therapeutic follow-up.

Graphical Abstract

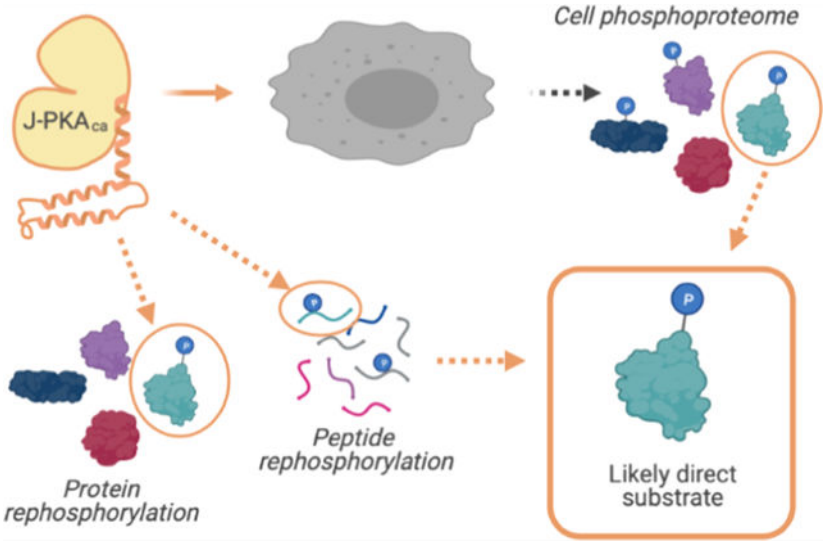

Keywords

fibrolamellar hepatocellular carcinoma; FL-HCC; protein kinase A; PKA; DNAJB1-PRKACA; phosphoproteomics; kinase inhibitors; kinase—substrate identification

INTRODUCTION

Fibrolamellar hepatocellular carcinoma (FL-HCC) is a primary liver cancer that occurs in young people without a gender bias or underlying liver diseases. It accounts for less than 1% of all primary liver cancers but represents the majority of HCCs in patients younger than 30 years of age.[1,2] Surgery is the mainstay of treatment in FL-HCC. No chemotherapeutic agents have been shown to have significant efficacy in HCC.[3] The gross anatomic feature of FL-HCC is an expanding, heterogeneous tumor mass with areas of increased vascularity and necrosis' including areas of fibrosis similar to focal nodular hyperplasia, a benign vascular-fibrotic lesion in the liver.[4]

Due to the rarity of FL-HCC and a lack of representative experimental systems, the molecular basis for carcinogenesis in these tumors has been elusive and difficult to study. Recently, however, there has been a breakthrough in understanding the pathogenesis and expression profile of the FL-HCC. Honeyman and colleagues discovered a novel, chimeric transcript that is present in all studied samples of FL-HCC.[5] Detection of a single, consistent

genetic deletion in one copy of chromosome 19[5,6] results in the formation of a chimeric gene, *DNAJB1 —PRKACA*, which combines the first exon of *DNAJB1*, the heat shock protein 40 (HSP40), with exons 2 through 10 of *PRKACA*, the catalytic subunit of protein kinase A (PKA_{ca}). This gives rise to a chimeric construct in which the N-terminal helix of PKA_{ca} is fused to the J-domain of DNAJB1 (J-PKA_{ca}). This chimera has been found to be the main driver of FL-HCC,[7] and while some of the changes downstream of its expression have been characterized, the detailed molecular pathogenesis producing those changes remains poorly understood.

PKA_{ca} is one of the best understood human kinases, and there is ample evidence to support the hypothesis that its kinase activity plays a role in FL-HCC.[5,6] Although protein kinases represent a significant class of potential drug targets, with more than 60 FDA-approved small-molecule kinase inhibitors and many more in development or in clinical trials[8,9] PKA itself seems to be a challenging target, likely due to its function in many normal cell types leading to dose-limiting toxicities and thus it may suffer from a narrow therapeutic window.[10] Furthermore, previous work has suggested that the catalytic activity of the chimeric fusion is not significantly different from that of the native PKA_{ca} enzyme,[5,7] yet the phenotypic differences observed in FL-HCC suggest that increased activity on native PKA_{ca} substrates is not the only contributor to oncogenic transformation; additional mechanisms may be activated by the chimera.[7] *DNAJB1* (otherwise known as HSP40) is a chaperone protein with numerous protein—protein interaction partners, and a recent study suggests that J-PKA_{ca} functions as a scaffold *via* its J (HSP40) component to assemble signaling elements that are then aberrantly phosphorylated by the catalytic portion of the chimera to contribute to the pathogenicity of FL-HCC.[11] Other recent work has characterized the allosteric effects of the J-domain on important aspects of the PKA activation mechanism, observing changes to the dynamics of the holoenzyme bound to regulatory subunits that impact important factors like cAMP binding, surfaces accessible for interaction with binding partners, and potentially localization.[12] Consequently, understanding the downstream pathways activated by excess WT PKA_{ca} activity *vs* aberrant J-PKA_{ca} chimera signaling may help to find new viable drug targets for FL-HCC. However, both PKA and HSP40 are upstream of a very broad set of cellular pathways, and their downstream effects are governed by particular regulatory interactions that determine substrates under a given set of biological conditions. Therefore, identifying particular direct substrates of both WT PKA_{ca} and the J-PKA_{ca} chimera in cells would be valuable for follow-up on candidate pathways for therapeutic intervention.

Many high-throughput approaches for the identification of phosphopeptides with mass spectrometry-based proteomics have been described (some reviewed in ref 13), but these do not typically enable clear assignment of direct substrates relative to those that may have been phosphorylated by other kinases downstream of the target kinase's activation. We seek to understand whether this chimeric fusion between HSP40 and PKA results in direct phosphorylation of a different set of substrates that could lead to its activation of unique pathways. Therefore, in the present study, we have employed an integrated strategy termed kinase assay linked with phosphoproteomics (KALIP)[14–17] (similar to other approaches employing cell lysates as a substrate pool for *in vitro* kinase reactions[18,19]) for comparing the specificity and identifying direct substrates of WT PKA_{ca} and the chimeric mutant

J-PKA$_{ca}$ (Figure 1). We identified phosphopeptides from cells overexpressing WT PKA$_{ca}$ or J-PKA$_{ca}$ (Figure 1A), as well as from *in vitro* kinase reactions with recombinant, purified WT PKA$_{ca}$ or J-PKA$_{ca}$ using either digested peptides (Figure 1B) or whole proteins as (Figure 1C) the substrate pool. These experiments identified some phosphosites associated uniquely with the chimeric fusion enzyme and enabled system analyses that revealed similarities and differences in the phosphosite motifs and pathways activated in the presence of the WT PKA$_{ca}$ *vs* J-PKA$_{ca}$. We also examined the differential WT PKA$_{ca}$ and J-PKA$_{ca}$ phosphoproteomes in response to two different PKA inhibitors in cells, identifying pathways and substrates that seemed to persist despite the apparent inhibition of other substrates and pathways. Overall, these findings of direct substrates, and substrates with differential inhibitor responses, could assist in prioritizing candidates for next-generation treatment of FL-HCC.

MATERIALS AND METHODS

Recombinant Enzyme Expression and Purification

High-level expression of human PKA$_{ca}$ and J-PKA$_{ca}$ in *Escherichia coli* was achieved by the construction of pET28a (+) vector that contained the protein gene subcloned prior to a phage T7 RNA polymerase promoter. Each species was expressed in the *E. coli* cell line BL21(DE3) by growing the bacteria in LB medium at 37 °C. Protein expression was induced by the addition of 0.4 mM IPTG and carried out overnight at 24 °C before harvesting the cells. Affinity purification was carried out using a Ni-NTA affinity resin (Thermo Scientific HisPur Ni-NTA Resin, catalogue number: 88221). Protein molecular weight was confirmed by SDS-PAGE (Figure S1). The activity of purified enzymes was confirmed by the PepTag nonradioactive protein kinase assay (Promega, catalogue number: V5340) (Figure S2).

Human Cell Culture and Transfection

Human embryonic kidney 293 cells (HEK293-T) were maintained in modified Dulbecco's medium (DMEM) supplemented with 10% fetal bovine serum, 100 μg/mL of streptomycin, and 100 IU/mL of penicillin in 5% CO_2 at 37 °C. Cells were grown to 80—90% confluency and then transiently transfected using the Lipofectamine 3000 transfection kit (Thermo Fisher Scientific) with 10 μg of plasmid containing either human PRKACA gene (pcrDNA3.1-PRKACA, Addgene plasmid #100890), DNAJB1—PRKACA gene (pcrDNA3.1-Chimera, Addgene plasmid #100891), or empty pcrDNA3.1 vector. Both plasmids were gifts from Sanford Simon.[5] Cells were incubated with plasmids for 36 h at 37 °C and 5% carbon dioxide in transfection media (DMEM/10% FBS) and then either harvested directly or treated with 0.1 mM sodium pervanadate for 15 min at 4 °C prior to harvesting. The cells were then washed twice with PBS, and the pellets were frozen at −80 °C until further processing as described in the Sample Preparation from Cell Lysates section. Sample aliquots were used to verify kinase expression *via* Western blotting, as described in the Supporting Information.

Inhibitor Treatment

Cells were maintained in modified Dulbecco's medium (DMEM) supplemented with 10% fetal bovine serum, 100 μg/mL of streptomycin, and 100 IU/mL of penicillin in 5% CO_2 at 37 °C and grown to ~80% confluency before transfection with plasmids as described above. Small-molecule inhibitor rpcAMPs (cAMPs-Rp triethylammonium salt, Tocris, Cat. #1337) (370 μM) was added with transfection (36 h of total treatment) or after 12 h of transfection (24 h of total treatment); cell-permeable peptide inhibitor PKI (myristoylated $PKI_{14–22}$ amide, Tocris, Cat. #2546) (6.4 μM) was added 12 h after transfection (24 h of total treatment). The cells were harvested after a total of 36 h in transfection media (DMEM/10% FBS). Cells were briefly pulsed with 0.1 mM sodium pervanadate for 15 min at 4 °C prior to harvesting the cells to inhibit phosphatase activity and prevent peptide dephosphorylation to "lock" phosphorylation sites in place for downstream analysis. The cells were then washed twice with PBS, and pellets were frozen at −80 until further processing, as described in the Sample Preparation from Cell Lysates section.

Sample Preparation from Cell Lysates

For all experiments except the native protein rephosphorylation, peptides were prepared as previously described:[20] cell pellets that had been snap-frozen at −80 °C were solubilized in lysis buffer (20% acetonitrile, 7 M urea, 2 M thiourea, 0.4 M TEAB, 4 mM DTT, phosphatase inhibitor cocktail (Pierce Phosphatase Inhibitor Mini Tablets, catalogue number: A32957), and Roche cOmplete, Mini EDTA-free Protease Inhibitor Cocktail 04693159001) and probe-sonicated to shear DNA. The cell debris was cleared by centrifugation at 16 000*g* for 30 min at 4 °C, and the supernatant containing the soluble proteins was collected. Protein concentrations were measured using the Bradford assay, and the lysate containing ~1 mg of total protein was reduced using TCEP (5 mM) and alkylated with iodoacetamide (40 mM) for 1 h at room temperature in the dark. Proteins were then digested with proteomics-grade trypsin (Pierce Trypsin Protease, MS grade-catalogue number 90058) at a ratio of 1:50 by mass (trypsin/total protein in lysate) overnight at 37 °C. On the next day, samples were acidified with 10% trifluoroacetic acid (TFA), desalted with Waters Oasis HLB cartridges, and concentrated to dryness using a Speed-Vac.

For the native protein rephosphorylation experiments, cell lysates were prepared in lysis buffer containing 50 mM Tris·HCl, pH 7.5, 150 mM NaCl, 5 mM EDTA, 1% Nonidet P-40, and protease inhibitor cocktail for 20 min on ice. Cell debris was cleared using centrifugation at 16 000*g* and 4 °C for 15 min. The supernatant containing soluble proteins was collected and measured for protein concentration and used in native protein rephosphorylation experiments as described below.

Phosphopeptide Enrichment

Sequential enrichment by metal oxide affinity chromatography (SMOAC) (Thermo Fisher Scientific) was used to enrich phosphopeptides according to the manufacturer's instructions. This method uses a two-step consecutive enrichment of phosphopeptides using TiO_2 and Fe-NTA spin columns.[21] The recovered phosphopeptides from this step were concentrated to dryness using a Speed-Vac.

Kinase Reactions for Rephosphorylation

For Peptide Rephosphorylation.—Peptide digests were prepared as described above. Samples were then resuspended in 100 μL of lambda phosphatase reaction buffer (50 mM Hepes, 100 mM NaCl, 2 mM DTT, 1 mM $MnCl_2$, pH 7.5). Lambda phosphatase (New England Biolabs P0753S) was added to each sample (2800–3000 units) and incubated overnight at 30 °C. The phosphatase was deactivated by heating at 75°C for 10 min. Samples were incubated in a kinase assay reaction buffer (100 mM Tris–HCl pH 7.8, 10 mM $MgCl_2$, 5 mM DTT, 2 mM ATP) containing the purified recombinant kinase (approximately 5000 units; estimated by *in vitro* kinase reaction with the recombinant, purified enzyme and relative quantification of bands *via* PepTag Nonradioactive protein kinase assays; Figure S2) at 30 °C for 90 min. Reactions were quenched by the addition of 0.5% TFA to a pH below 3. The samples were then desalted using Waters HLB cartridges and concentrated to dryness using a Speed-Vac.

For Native Protein Rephosphorylation.—Samples (2 mg of total protein in 300 μL of lysis buffer each) were treated with lambda phosphatase (2800–3000 units) in phosphatase buffer (500 mM Tris–HCl, pH 7.5, 1 mM Na_2 EDTA, 50 mM dithiothreitol) and 2 mM Mn ion ($MnCl_2$) and incubated at 37 °C for 90 min. Since it was preferred to keep the proteins in their native, folded state, heat inactivation was not desirable; therefore, to stop the reaction, a cocktail of two tablets of phosphatase inhibitor (Pierce Phosphatase Inhibitor Mini Tablets, catalogue number: A32957) and two tablets of protease inhibitor (Roche cOmplete, Mini, EDTA-free Protease Inhibitor Cocktail #04693159001) dissolved in 5 ml of kinase reaction buffer was prepared and 150 μL of this cocktail was added to each sample, stirring gently with a small magnetic stirrer while holding in a water bath for 10 min. A fraction of the reaction was kept as control for MS analysis, and for rephosphorylation reaction, the purified recombinant kinases (~5000 units, estimated as described above for peptide rephosphorylation) were added to each sample in kinase buffer (20 mM potassium phosphate, 180 mM KCl, 20 mM $MgCl_2$, 5 mM DTT, and 200 μM ATP) while gently stirring (as above) for 60 min at 30 °C. The kinase reaction was quenched by heat inactivation (75 °C for 10 min) and dialyzed overnight against trypsin digestion buffer (100 mM Tris–HCl, 10 mM $CaCl_2$, 5 mM DTT, pH 7.8) in Pur-a-lyzer midi dialysis tubes (Sigma-Aldrich PURD10005) for buffer exchange, resulting in a minimal amount of protein precipitation. Samples were then resolubilized using up to 2 M urea, alkylated with iodoacetamide, digested using trypsin, desalted and concentrated to dryness, and phosphoenriched using the SMOAC strategy as described for other samples above.

Mass Spectrometry Data Acquisition and Data Analysis

The phosphopeptide samples were then analyzed by LC-MS/MS as previously[20] using a Thermo Scientific Easy NanoLC LC 1000 system coupled to a high-resolution Orbitrap Fusion Tribrid Mass Spectrometer using a reverse phase C18 column with a 60 min linear gradient of 2–30% B (solvent A: water +.01% formic acid; solvent B: acetonitrile+.01% formic acid) at a flow rate of 200 nL/min. The mass spectrometer was operated in a data-dependent mode with a resolution of 60 000 and a scan range of 300–1500 m/z. The top 12 most abundant ions were selected with a dynamic exclusion time of 15 s for high collision dissociation (HCD), and fragments were analyzed.

Raw data files were processed for peptide, protein, and phosphosite identification using PEAKS Studio XPro software (Bioinformatics Solutions Inc.) against the complete UniProt human reference proteome (containing both reviewed and unreviewed entries). Details of phosphorylation sites per protein were extracted from the exported PEAKS PTM search result tables for further comparisons and analyses using a custom-built PHP script we named PEAKS-ModExtractor (https://gitlab.com/jackbrennan07/peaks-modextractor). Instructions for using Peaks-ModExtractor are available at the link provided.

Qualitative Data Analysis to Identify Shared and Unique Sites (Cell-Based Phosphoproteomic Profiling, *In Vitro* Rephosphorylation, and Cell-Based Inhibitor Experiments).—For all experiments, lists of phosphopeptides/phosphorylation sites identified were analyzed qualitatively to extract a final list of sequences/sites that were identified robustly and compared to each other to determine which were shared and which were uniquely present in a given experiment: first, during the PEAKS Studio Xpro export process, a false discovery rate (FDR) cutoff for peptide identification was applied and only peptides with FDR ≤ 1% were included. Next, results from PEAKS-ModExtractor outputs were filtered to include only those with Ascore values ≤30. This value was selected as a cutoff based on the previously published evaluation of the Ascore metric performance,[22,23] which demonstrated that phosphopeptides with Ascores above this cutoff are reliably high confidence for identifying and localizing the modification. Then, data sets from each experiment were compared using BioVenn (http://www.biovenn.nl/index.php)[24] and additionally filtered to focus on more robust observations by only including phosphopeptides observed in both replicates. The resulting lists were then qualitatively background-subtracted (also using BioVenn) by removing any sites that were also identified in the experiment's respective negative control (the empty vector-only control for the cell-based experiments and phosphatase-treated inputs for the *in vitro* rephosphorylation experiments). As a further approach to ensure interpretation of the identified peptides/proteins in context, we included a reference table from the CRAPome,[25] a repository of proteins commonly identified across many affinity purification mass spectrometry (AP-MS) experiments compiled at and downloaded from https://reprint-apms.org, and provided information about how often a given protein has been observed (via average spectral counts across CRAPome experiments) with our results listed in Supporting Table S1. It should be noted that this CRAPome reference is not from phosphopeptide enrichment by SMOAC and therefore may not fully represent the type of background contaminants relevant to this experiment —however, it may still be a useful reference for considering the cellular context of different protein abundances and the nature of different types of binding interactions relevant to our result list.

Comparing Tryptic Peptides *vs* Sites in Their Protein Context.—Peptide sequences pulled from the PEAKS result tables by PEAKS-ModExtractor were used to compare results from the peptide rephosphorylation experiment; however, because phosphorylation at the protein level (i.e., in cells and in the native protein rephosphorylation experiment) occurred before protease digestion, the identified peptide lists were not sufficient to analyze substrate motifs. Thus, phosphorylation site(s) per protein identifier were used to retrieve the sequences surrounding the identified phosphosites (−7 to +7) by

retrieving protein region sequence information from UniProt *via* the Retrieve/ID Mapping function, downloading the results as noncompressed “source list”.fasta files. The resulting consolidated lists of 15 AA sequences −7 to +7 from each phosphorylation site were used for comparison analyses. Motif visualization was performed using PTM-Logo.[26] Sequences of <15 or >15 amino acids in length (arising from, e.g. isoform conflicts, redundant partial sequences in unreviewed entries, etc.) were excluded from PTM-logo motif analysis due to limitations of the motif tool. In cases where nonuniform sequences needed to be evaluated (e.g. the peptide rephosphorylation experiment), the Weblogo resource was used.[27]

Raw data, associated PEAKS result files, and PEAKS-ModExtractor outputs are available for download at the MassIVE repository (https://massive.ucsd.edu, accession #MSV000086707).

RESULTS

Cell-Based Phosphoproteomics Profiles and Signaling Pathway Comparison

To compare the signaling profiles of WT PKA_{ca} and its oncogenic mutant J-PKA_{ca}, constructs containing each protein were transiently expressed in HEK293 cells in duplicate. Cells transfected with empty vectors were used as a control. Expression levels were verified by Western blot against the human cAMP-dependent protein kinase A catalytic subunit, which recognizes both WT PKA_{ca} and J-PKA_{ca} (Figure S1). It should be noted that the expression of both WT- and J-PKA_{ca} were relatively high in the cell line model and may have resulted in differences in ratios of catalytic to regulatory subunits that would affect the physiological behavior of the kinase activation. Cells were treated briefly with the phosphatase inhibitor pervanadate to enhance phosphorylation site stability for downstream analysis and lysed in denaturing lysis buffer. Phosphopeptides were enriched using sequential metal oxide affinity chromatography (SMOAC), as described in the Materials and Methods section, and analyzed on an Orbitrap Fusion LC-MS/MS. Mass spectrometry data were processed using PEAKS Studio XPro, and modified peptides were extracted from the PTM search export using PEAKS-ModExtractor. The outputs were filtered to ignore modifications other than phosphorylation of STY and Ascore values below 30. To control for background phosphorylation, phosphosite identifications from the vector-only control were filtered from the sites identified in WT PKA_{ca}- and J-PKA_{ca}-expressing cells. These background-subtracted lists were used to make phosphosite comparisons between replicates and conditions.

Overall, 3195 phosphosites were confidently identified in both replicates from WT PKA_{ca}-expressing cells and 2616 from J-PKA_{ca}-expressing cells. After filtering out those that were also observed in the vector control, 1244 were unique to WT PKA_{ca}, 809 to J-PKA_{ca}, and 770 were common between the two (Figure 2A). Pathway activation was evaluated using ingenuity pathways analysis (IPA) in the phosphorylation analysis mode for each phosphosite list from WT PKA_{ca}- and J-PKA_{ca}-expressing cells and also for phosphosites identified as higher abundance in tumor *vs* adjacent normal tissues (>1 $\log_2$-fold change or only in tumors) from a recent phosphoproteomics study of FL-HCC patient samples.[11] Full pathway analysis tables are available in the Supporting Information. Some of the pathways observed as significantly enriched in the overexpression cell lines were likely cell-

type-specific, as they were not observed as activated from the patient sample data. However, a number of substrates and key pathways enriched in the FL-HCC patient sample data were also observed in WT PKA_{ca}- and J-PKA_{ca}-expressing cells (Figure 2B,D), in particular, the ERK/MAPK signaling pathway that was identified as important in the patient sample study by Turnham et al. These results support that despite the caveat related to the ratio of catalytic to regulatory subunit expression levels, it seems reasonable to use HEK293 cells overexpressing the kinase constructs as model systems for examining direct substrates of these kinases in this context. However, they also suggest that most of the pathway activation may arise broadly from overactive PKA and not necessarily from substrate interactions unique to the DNAJB1/HSP40 chaperone interactions, given that pathways activated in WT PKA_{ca}-expressing cells were overall the same as in J-PKA_{ca}-expressing cells. The only pathways with stronger enrichment in J-PKA_{ca}-expressing cells *vs* WT PKA_{ca} included EIF2 signaling, protein ubiquitination, and aldosterone signaling in epithelial cells (Figure 2D), none of which were very highly enriched in the patient sample data. With respect to specific phosphorylation sites, direct comparisons of the HEK293 cell overexpression models with the patient FL-HCC data are subject to the caveat that the phosphoenrichment technique, instrumentation, peptide identification software, and human proteome databases were not the same; however, there were nevertheless still some sites observed in common (Figure 2B).

The sequences surrounding the overlapping sites (Table 1) were further examined. The amino acid motif around most of the 39 phosphorylation sites observed in common among the FL-HCC tumor>normal, J-PKA_{ca}, and WT PKA_{ca} data sets showed similar characteristics to that seen for direct phosphorylation of proteins by recombinant WT PKA_{ca} in experiments reported by Sugiyama et al.[28] (Figure 2C), suggesting that many of these sites are likely to be direct substrates in FL-HCC that arise from abnormal levels of PKA activity. Intriguingly, the 21 sites that were observed in common only in FL-HCC tumor > normal/J-PKA_{ca} exhibited the expected enrichment of hydrophobic amino acids at +1, whereas the 28 sites shared only in FL-HCC tumor>normal/WT PKA_{ca} did not. This suggests that the 21 FL-HCC tumor > normal/J-PKA_{ca} sites may also represent unique direct substrates of the J-PKA_{ca} mutant, while those observed as unique in the WT PKA_{ca} data may be more likely to be downstream and not direct. This was also supported by direct phosphorylation experiments (as described below and in Table 2).

Identification of Direct *In Vitro* Substrates of PKA_{ca} and J-PKA_{ca} Using HEK293 Cell Line Models

We were interested in determining which of the phosphorylation sites observed in our experiments were most likely direct substrates of either J-PKA_{ca} and/or WT PKA_{ca}. PKA is known to phosphorylate a number of motifs that have variations on the basic R/K-R/K-X-S/T motif, including R-X-R-R-X-S-Φ (where Φ is a hydrophobic residue), R-R-X-S-Φ, and R-R-X-S/T;[29] however, these motifs are very simplistic and generic, with insufficient information about the full range of amino acids,especially C-terminal to the phosphosite, to adequately facilitate identification of direct substrates from cell-based phosphosite profiles. To explore this, we chose the Kinase Assay LInked with Phosphoproteomics (KALIP) approach,[14,16,20] in which cell lysates from the HEK293 kinase construct overexpression

models were used as substrate pools for rephosphorylation by purified kinase *in vitro* (as illustrated in Figure 1). This provided a more relevant comparison to the phosphosite profiles we observed from cell-based phosphoproteomics described in the previous section. Previously, in the work by Sugiyama et al., PKA was one of >360 kinases profiled for phosphorylation of whole-protein substrates *in vitro*, using HeLa cell lysate as the substrate pool.[28] In that work, cell lysates prepared in a nondenaturing buffer were treated with phosphatase to remove pre-existing phosphate groups and then heated to 75 °C to inactivate the phosphatase, which also could have denatured many of the proteins.[30] We were most interested in maintaining the native structural states of the proteins and avoiding heat treatment, so we used whole-protein lysate from the cells overexpressing J-PKA_{ca} or WT PKA_{ca} as the substrate pool after inactivating the phosphatase using phosphatase inhibitors. However, heat treatment would have also denatured endogenous kinases that may produce background phosphorylation; since we did not heat-treat, those kinases may have still been active. This led to the caveat that some observations may not result from direct phosphorylation. Accordingly, we also performed KALIP rephosphorylation on the trypsin digest of the lysate from cells overexpressing J-PKA_{ca} or WT PKA_{ca}, which was subject to its own caveat that trypsin digest would disrupt the N-terminal R/K motifs typically present in PKA substrates. However, by combining the information from these two experiments, we were able to balance the caveats of each to learn more about the C-terminal substrate motifs independent of the optimal N-terminal motif, confirm the amino acid patterns seen for +1 to +4 in the work from Sugiyama et al., compare substrate profiles for J-PKA_{ca} and WT PKA_{ca}, and cross-reference for sites also observed in FL-HCC tumor tissues by Turnham et al.[11]

Peptide Rephosphorylation.—Considering only the peptides robustly identified in both kinase reaction replicates, 188 phosphopeptides were observed for the J-PKA_{ca} *vs* 96 for the WT PKA_{ca} in the peptide rephosphorylation experiments and 120 phosphorylation sites on 96 proteins for J-PKA_{ca} *vs* 116 sites on 99 proteins for WT PKA_{ca} in the protein rephosphorylation experiments. In general, the phosphorylation motifs observed in the peptide experiment matched the known hydrophobic motif-S-Φ-Φ-C-terminal to the phosphorylation site, which several studies (including an expressed oriented peptide library consisting of S-centered sequences from human proteins reported by the Rinehart and Turk, as well as the protein rephosphorylation study by Sugiyama et al.) have previously reported.[19,28] The vast majority of the sequences surrounding the sites were truncated in the tryptic digest that was used for peptide rephosphorylation, with very little missed cleavage; thus, the peptides themselves in the kinase reaction did NOT have the common N-terminal -(R/K)-(R/K)-X-S-motif. However, interestingly, when mapped back to the context of their full proteins, the sites phosphorylated still largely contained the N-terminal positively charged residues (R/K) at −2 and −3 (Figure 3B). We speculate that perhaps this reflects the evolution of direct PKA substrates as containing both N- and C-terminal components of the motif and that the motif on the C-terminal side of the phosphosite is to some degree sufficient to direct PKA phosphorylation as seen in our peptide rephosphorylation experiment. Further, a much larger number of unique phosphopeptides were seen for the J-PKA_{ca} peptide reaction, and the sequence motif for those was slightly different from that for the shared and WT PKA_{ca}-unique sequences, showing less enrichment of hydrophobic

amino acids at +2 and more acidic amino acids at +3. These differences suggest some intrinsic distinctions in substrate recognition of J-PKA$_{ca}$ *vs* WT PKA$_{ca}$— for example, this may indicate that J-PKA$_{ca}$ substrate recognition is less reliant on the N-terminal basic amino acid motif, with the C-terminal motif being sufficient for phosphorylation by the mutant. It could also mean that the J-domain alters catalytic dynamics in a way that depends more on the C-terminal motif and leads to increased turnover for more substrates, which may not be reflected in the K_m or V_{max} values previously characterized using a limited set of substrates that all contained the N-terminal basic motif.[31,32]

Protein Rephosphorylation.—For the protein rephosphorylation experiments, the background phosphorylation by nondenatured kinases in the cell lysate is evident from the sequence motifs observed (Figure 3C); however, several were also identified by Sugiyama et al.[28] (see Supporting Table S2) and/or as higher in FL-HCC tumor than in normal tissue by Turnham et al.[11] (Supporting Table S1), which did exhibit the expected PKA N- and/or C-terminal motifs. These observations suggest that those sites also identified in Turnham et al.[11] are likely to be bona fide direct substrates of J-PKA$_{ca}$ and/or WT PKA$_{ca}$ in FL-HCC tumor tissues (summary of these proteins is shown in Table 2).

Both Peptide and Protein Rephosphorylation.—Twenty-two phosphosites were identified in common in both the peptide and protein experiments (17 sites for J-PKA$_{ca}$ and 12 sites for WT PKA$_{ca}$). Of those, 10 were unique to J-PKA$_{ca}$, 5 to WT PKA$_{ca}$, and 7 were common between both (Figure 3A). Three of the sites in common sites were also seen as higher in tumor than normal in FL-HCC tissues[11] (Table 2): the DNA repair protein XRCC6/Ku70 (Ku70 S520), 60S ribosomal protein L3 (RPL3 S13), and triosephosphate isomerase (TPIS S21). All three of these sites have been reported to be phosphorylated in many prior studies (as curated in the PhosphoSitePlus database, https://phosphosite.org); RPL3 S13 and TPIS S21 were also observed in the PKA protein rephosphorylation experiment performed by Sugiyama et al.; however, they have not been studied in depth as PKA substrates, and Ku70 S520 has not been previously associated with PKA.

Phosphoproteomics of Inhibitor-Treated Cells Expressing J-PKA$_{ca}$ or WT PKA$_{ca}$

We were also interested in how PKA inhibitors would affect the phosphorylation profile in cells expressing chimeric J-PKA$_{ca}$ *vs* the WT PKA$_{ca}$. We applied two PKA inhibitors with different inhibition mechanisms, rpcAMPs and a truncated, myristoylated form of protein kinase A inhibitor peptide (PKI$_{14–22}$) (Figure 4). rpcAMPs competitively inhibit the cAMP-induced activation of the kinase by binding to the regulatory subunit (best characterized for RIα) and stabilizing the inactive conformation of the PKA$_{ca}$ catalytic subunit in the holoenzyme,[33,34] while PKI is an endogenous peptide that competitively inhibits substrate binding to the catalytic subunit.[31,35] Cells overexpressing each version of the kinase were treated with each inhibitor in culture across different points in the time line between transfection and harvesting (Figure 4B); lysates were harvested in the presence of phosphatase inhibitor, and phosphopeptides were enriched and identified by LC-MS/MS. Two incubation time span experiments were performed for rpcAMPs (36 h coincubation for the entire transfection time line and addition after 12 h from transfection for 24 h inhibitor treatment). PKI was added after 12 h for a 24 h inhibitor treatment to minimize any

potential effects of peptide biostability on the results; myristoylated $PKI_{14–22}$ has been used in cell-based experiments as long as 24–96 h;[36,37] therefore, 24 h should be well within its biostability window. Both inhibitors resulted in a noticeable reduction of phosphopeptides for PKA_{ca} and J-PKA_{ca} (Figure 4C); however, full 36 h cotreatment with rpcAMPs during the course of J-PKA_{ca} overexpression was also associated with observation of a substantial number of new phosphopeptides not seen in the -inh control. Further, a subset of certain phosphopeptides seemed to persist in cells expressing each version of the kinase even in the presence of each inhibitor (Figure 4C and Table 3), with additional subsets persisting in PKI-treated cells or in rpcAMP-treated cells through both time points (see Supporting Table S1 for full lists).

It is difficult to confidently evaluate the motifs for phosphosites that were not observed in the presence of inhibitor *vs* the control since the absence of evidence is not necessarily evidence of absence (particularly for mass spectrometry of peptides). However, it is useful to evaluate the sequence characteristics for the sites that were consistently observed across conditions. We found some interesting differences in the motifs observed for phosphosites that persisted in the presence of different inhibitors with each kinase construct (Figure 5). Generally, the sites that persisted in the presence of both inhibitors that were either unique for J-PKA_{ca} or shared for both kinase constructs exhibited motifs that were more similar to the known substrate preference motif (K/R at −2 and/or −3 and hydrophobic residues at +1 and/or +2) and were different from those persisting only in the WT PKA_{ca} inhibitor experiments (Figure 5A). Also, a larger number of persistent sites were seen uniquely for J-PKA_{ca} than for WT PKA_{ca}. This might indicate that J-PKA_{ca} is more resistant to inhibition *via* either mode (substrate-competitive and regulatory subunit stabilization, as illustrated in Figure 4A). Differences were seen for which sites persisted in the presence of PKI *vs* rpcAMPs, as well. The number of sites that persisted through PKI treatment was greater for the WT PKA_{ca}-expressing cells than for J-PKA_{ca}, although the motifs were not very different (when generalized to polarity) and were not very similar to PKA substrate preference motifs; also, very few sites persisted in the presence of rpcAMPs but not PKI for WT PKA_{ca}. On the other hand, a much larger number of sites persisted through rpcAMP treatment in J-PKA_{ca}-overexpressing cells than for WT PKA_{ca}, and the sequences around those sites closely resembled the PKA substrate motif. This may suggest that rpcAMP, in particular, is less effective at J-PKA_{ca} inhibition, while PKI inhibition of the chimeric form is not as impacted.

DISCUSSION

PKA signaling is involved in the control of a wide variety of cellular processes from metabolism to ion channel activation, cell growth and differentiation, gene expression, and apoptosis. The J-PKA_{ca} hallmark mutation in FL-HCC seems to affect these processes in complex ways that go beyond straightforward amplification of normal PKA pathways, including novel activation of Wnt/β-catenin, Ras–Raf–Erk pathways, and others,[7,11] and also seems to evade the regulatory control of endogenous inhibitors like the PKI peptides, despite the expression of those inhibitors in tumor cells and a lack of difference in biochemical inhibition by various forms of PKI *in vitro* for J-PKA_{ca} *vs* WT PKA_{ca}.[31] So far, although pathways have been characterized and some upstream/downstream kinase

activation has been predicted,[11] the direct kinase–substrate relationships that lead to these signaling outcomes have not been identified, and the molecular mechanisms by which J-PKA$_{ca}$ promotes oncogenesis in FL-HCC are still not fully understood. While the work described here does not comprehensively map or prove these mechanisms, it provides evidence for potential direct substrates that may be important to pursue in the future.

Disrupted Regulatory Interactions *vs* Unique Downstream Substrate/Pathway Activation

Turnham et al. proposed that the J-domain/HSP40 promotes aberrant interactions with novel substrates through its chaperone functions.[11] Other recent work has proposed that changes to the allosteric connectivity in the kinase resulting from the J-domain fusion affect the ability of the chimeric version of the kinase to interact with its regulatory domains, leading to aberrant phosphorylation and activation of established PKA signaling pathways.[12,32] Our data contain evidence that supports both of these proposals, and our experiments are particularly helpful for comparing J-PKA$_{ca}$ with the WT kinase head-to-head. On the one hand, we observed overall that the pathways induced by expression of the J-PKA$_{ca}$ mutant were not substantially different from those induced by WT PKA$_{ca}$, and most of the phosphorylation sites we detected in J-PKA$_{ca}$-overexpressing cells that were shared with tumor *vs* normal FL-HCC tissue (Turnham et al.[11]) were also detected in WT PKA$_{ca}$-overexpressing cells. This suggests that for the most part, J-PKA$_{ca}$ overexpression produces very similar downstream outcomes as just overexpressing/overactivating PKA activity more generally, supporting the idea that the key differences lie in the regulation of PKA kinase activity and not necessarily in new substrates phosphorylated by the mutant. On the other hand, some specific phosphorylation sites we detected in J-PKA$_{ca}$-expressing cells, but not in WT, also support that there may be particular events related to the J-domain chimera, e.g., phosphorylation of KSR1 at S888, which is homologous to a PKA-phosphorylated site in murine KSR1 that has been linked to cAMP/PKA activation of the ERK1/2 cascade[38] (a pathway that was suggested as key to the J-PKA$_{ca}$ mechanism by Turnham et al.), and/or additional heat shock proteins by J-PKA$_{ca}$ (Tables 1 and 2). However, most of the J-PKA$_{ca}$-“unique” sites from each given experiment were also seen across various versions of the WT experiments, suggesting that they are not truly unique to the mutant. S423 of actinin-4 (ACTN4 S23) was the one apparently direct site that was seen in all three J-PKA$_{ca}$ experiments, but only in WT PKA$_{ca}$ peptide rephosphorylation and not the corresponding WT protein rephosphorylation and cell experiments; this site was also higher in tumor *vs* normal in FL-HCC and may be worth additional study, given the ACTN4’s role in malignancy and metastasis.[39]

We also identified sites and pathways that were differentially affected by the PKA inhibitors rpcAMPs and PKI$_{(14–22)}$, leading to a set of phosphorylation sites that persisted in the presence of each inhibitor (Figures 4 and 5). While we cannot rule out the potential that overexpression of the catalytic domain to levels higher than can be sufficiently modulated by the regulatory subunit available in the cell, and many of the persistent substrates and pathways were common to both forms of the enzyme (Table 3), intriguingly some were not (Figure 5). The J-PKA$_{ca}$ chimera seemed to be particularly resistant to inhibition by rpcAMPs, which is consistent with the mechanism proposed by Lu et al. from cryo-EM structures of the holoenzyme,[12] in which the J-domain seems to affect the dynamics and

allostery of the regulatory subunit interactions, resulting in destabilization such that J-PKA$_{ca}$ is more easily activated by cAMP. It is plausible that destabilization of those regulatory subunit interactions could also destabilize interaction of the mutant holoenzyme with rpcAMPs and enable cAMP to compete more effectively for J-PKA$_{ca}$ binding, which would allow the mutant to retain higher activity in the presence of rpcAMPs at the concentrations used in our experiments. Also, the persistence of signaling pathways associated with pyrimidine biosynthesis and DNA damage response in J-PKA$_{ca}$-expressing cells in the presence of rpcAMPs (Figure 5D) further suggests that some unique mechanisms are present downstream of the mutant. Overall, our data should be useful to others for the study of the specific mechanisms that may govern aberrant activation resulting from amplification of PKA activity due to the J-domain fusion's disruption of regulatory complexes, as well as potential unique downstream pathways.

Candidate Direct Substrates That May Govern Pathogenesis in FL-HCC

A key goal of this study was to identify direct substrates of J-PKA$_{ca}$ that could be contributing to pathogenesis in FL-HCC. The KALIP workflow enabled us to determine a number of apparently direct substrates of both WT PKA$_{ca}$ and J-PKA$_{ca}$, including some that were also observed by others in FL-HCC tumor tissues[11] and that connect to pathways that are well supported by other studies. Two specific sites on two proteins were identified across all experiments (for mutant and WT kinase): S520 of XRCC6 (the DNA damage repair/nonhomologous end-joining-related protein Ku70) and S13 of RPL3 (a component of the 60S ribosome), strongly suggesting that they are direct substrates of both forms of the kinase. These sites were also persistent in the presence of inhibitors PKI and rpcAMPs. A number of other sites that were present in FL-HCC tissues were also apparently persistent in the presence of inhibitors in our experiments, and we saw evidence for direct phosphorylation by J-PKA$_{ca}$/WT PKA$_{ca}$ for some of these (Table 3). One potentially notable site observed as persistent to inhibitors for both J-PKA$_{ca}$ and WT was S58 on the regulatory subunit RIIα. This site is in a disordered region of the protein not visible in the published structures, but it has previously been observed in other phosphoproteomics studies[40–43] and is close to a CDK2 phosphorylation site (T54) that is important for regulation of PKA localization to the centrosome during mitosis.[41] According to STRING analysis,[44] several of the apparently direct sites are on proteins associated with either RPL3 or Ku70 in complexes involved in translational regulation (RPL3) or nonhomologous end-joining (NHEJ) (Ku70) (Figure 6A). This raises the interesting possibility that deregulated PKA signaling *via* these particular complexes may be important to FL-HCC pathogenesis but also difficult to target *via* PKA directly, so other potential druggable targets in those networks (e.g., DNA-PK or the ribosome) may be valuable for future FL-HCC therapeutic development.

Phosphorylation of the J-Domain at S16

In all of our experiments with J-PKA$_{ca}$, we observed that S16 of the J-domain was phosphorylated, and we also observed this in the rephosphorylation experiments. However, because we were introducing recombinant J-PKA$_{ca}$ in the kinase reaction, we cannot confirm that this is a direct autophosphorylation substrate of the mutant kinase, and this site was not reported in studies by Turnham et al.[11] Further, it was also detected in one run of the WT control experiment (albeit in a single replicate and at a level close to the noise,

far lower than in any J-PKA$_{ca}$ experiment and likely an artifact of MS analysis), so we are cautious about overinterpreting this phosphorylation site. Nevertheless, this site is located on the hinge region of the J-domain (Figure 6B), and it was observed as persistent in all of the J-PKA$_{ca}$ inhibitor experiments; given the importance of J-domain dynamics on the regulatory interactions described by other studies,[12,32] it is possible that this phosphorylation event is significant, and it may be worthwhile for future structural studies to take it into account.

CONCLUSIONS

Overall, we identified a number of phosphorylation sites that are associated with deregulated PKA activity in these overexpression model systems that also were rephosphorylated *in vitro* by recombinant enzyme, suggesting that they are direct substrates of either J-PKA$_{ca}$, WT PKA$_{ca}$, or both. Even though we used HEK293 cells as our model and FL-HCC is a liver cancer, a substantial number of the sites we detected were consistent with sites detected at higher levels in FL-HCC tissues *vs* normal, lending confidence to the relevance of these phosphorylation events to this cancer. While not comprehensive examinations of the pathophysiology of this disease, the data presented here provide potential lead mechanisms for further evaluation as targets. Of those we identified, some of the key players (DNA-PK and the ribosome) are currently being pursued as drug targets in preclinical and clinical studies, and candidate compounds may be available for testing sensitivity of this cancer type. Since safely inhibiting PKA activity itself is a challenging prospect, the potential targets presented here may represent more viable opportunities for therapeutic intervention in FL-HCC.

Supplementary Material

Refer to Web version on PubMed Central for supplementary material.

ACKNOWLEDGMENTS

This work was supported by the National Institutes of Health/National Cancer Institute through R01CA183571 (L.L.P.). The authors thank Sanford Simon for the expression plasmids used in this study. The table of contents graphic was created with BioRender.com. The authors also acknowledge John Blankenhorn for early data analysis iterations for the cell-based experiments in Protein Pilot 5.0 that were replaced by PEAKS Studio Xpro and not used in the final version of this manuscript.

REFERENCES

(1). Eggert T; McGlynn KA; Duffy A; Manns MP; Greten TF; Altekruse SF Fibrolamellar hepatocellular carcinoma in the USA, 2000–2010: A detailed report on frequency, treatment and outcome based on the Surveillance, Epidemiology, and End Results database. United Eur. Gastroenterol. J 2013, 1, 351–357.

(2). Torbenson M. Fibrolamellar carcinoma: 2012 update. Scientifica 2012, 2012, No. 743790.

(3). Ang CS; Kelley RK; Choti MA; Cosgrove DP; Chou JF; Klimstra D; Torbenson MS; Ferrell L; Pawlik TM; Fong Y; O'Reilly EM; Ma J; McGuire J; Vallarapu GP; Griffin A; Stipa F; Capanu M; Dematteo RP; Venook AP; Abou-Alfa GK Clinicopathologic characteristics and survival outcomes of patients with fibrolamellar carcinoma: data from the fibrolamellar carcinoma consortium. Gastrointest. Cancer Res 2013, 6, 3–9. [PubMed: 23505572]

(4). Andersen JB Fibrolamellar hepatocellular carcinoma: a rare but distinct type of liver cancer. Gastroenterology 2015, 148, 707–710. [PubMed: 25724459]

(5). Honeyman JN; Simon EP; Robine N; Chiaroni-Clarke R; Darcy DG; Lim II; Gleason CE; Murphy JM; Rosenberg BR; Teegan L; Takacs CN; Botero S; Belote R; Germer S; Emde AK; Vacic V; Bhanot U; LaQuaglia MP; Simon SM Detection of a recurrent DNAJB1-PRKACA chimeric transcript in fibrolamellar hepatocellular carcinoma. Science 2014, 343, 1010–1014. [PubMed: 24578576]

(6). Darcy DG; Chiaroni-Clarke R; Murphy JM; Honeyman JN; Bhanot U; LaQuaglia MP; Simon SM The genomic landscape of fibrolamellar hepatocellular carcinoma: whole genome sequencing of ten patients. Oncotarget 2015, 6, 755–770. [PubMed: 25605237]

(7). Kastenhuber ER; Lalazar G; Houlihan SL; Tschaharganeh DF; Baslan T; Chen CC; Requena D; Tian S; Bosbach B; Wilkinson JE; Simon SM; Lowe SW DNAJB1-PRKACA fusion kinase interacts with beta-catenin and the liver regenerative response to drive fibrolamellar hepatocellular carcinoma. Proc. Natl. Acad. Sci. U.S.A 2017, 114, 13076–13084. [PubMed: 29162699]

(8). Ferguson FM; Gray NS Kinase inhibitors: the road ahead. Nat. Rev. Drug Discovery 2018, 17, 353–377. [PubMed: 29545548]

(9). Roskoski R. FDA-approved small molecule protein kinase inhibitor compilation. http://www.brimr.org/PKI/PKIs.htm.

(10). Propper DJ; Saunders MP; Salisbury AJ; Long L; O'Byrne KJ; Braybrooke JP; Dowsett M; Taylor M; Talbot DC; Ganesan TS; Harris AL Phase I study of the novel cyclic AMP (cAMP) analogue 8-chloro-cAMP in patients with cancer: toXicity, hormonal, and immunological effects. Clin. Cancer Res 1999, 5, 1682–1689. [PubMed: 10430069]

(11). Turnham RE; Smith FD; Kenerson HL; Omar MH; Golkowski M; Garcia I; Bauer R; Lau HT; Sullivan KM; Langeberg LK; Ong SE; Riehle KJ; Yeung RS; Scott JD An acquired scaffolding function of the DNAJ-PKAc fusion contributes to oncogenic signaling in fibrolamellar carcinoma. eLife 2019, 8, No. e44187.

(12). Lu TW; Aoto PC; Weng JH; Nielsen C; Cash JN; Hall J; Zhang P; Simon SM; Cianfrocco MA; Taylor SS Structural analyses of the PKA RIIbeta holoenzyme containing the oncogenic DnaJB1-PKAc fusion protein reveal protomer asymmetry and fusion-induced allosteric perturbations in fibrolamellar hepatocellular carcinoma. PLoS Biol. 2020, 18, No. e3001018.

(13). Bodenmiller B; Aebersold R. Quantitative analysis of protein phosphorylation on a system-wide scale by mass spectrometry-based proteomics. Methods Enzymol. 2010, 470, 317–334. [PubMed: 20946816]

(14). Xue L; Arrington JV; Tao WA Identification of Direct Kinase Substrates via Kinase Assay-Linked Phosphoproteomics. Methods Mol. Biol 2016, 1355, 263–273. [PubMed: 26584932]

(15). Xue L; Geahlen RL; Tao WA Identification of direct tyrosine kinase substrates based on protein kinase assay-linked phosphoproteomics. Mol. Cell. Proteomics 2013, 12, 2969–2980. [PubMed: 23793017]

(16). Arrington J; Xue L; Wang WH; Geahlen RL; Tao WA Identification of the Direct Substrates of the ABL Kinase via Kinase Assay Linked Phosphoproteomics with Multiple Drug Treatments. J. Proteome Res 2019, 18, 1679–1690. [PubMed: 30869898]

(17). Xue L; Wang WH; Iliuk A; Hu L; Galan JA; Yu S; Hans M; Geahlen RL; Tao WA Sensitive kinase assay linked with phosphoproteomics for identifying direct kinase substrates. Proc. Natl. Acad. Sci. U.S.A 2012, 109, 5615–5620. [PubMed: 22451900]

(18). Kettenbach AN; Wang T; Faherty BK; Madden DR; Knapp S; Bailey-Kellogg C; Gerber SA Rapid determination of multiple linear kinase substrate motifs by mass spectrometry. Chem. Biol 2012, 19, 608–618. [PubMed: 22633412]

(19). Barber KW; Miller CJ; Jun JW; Lou HJ; Turk BE; Rinehart J. Kinase Substrate Profiling Using a Proteome-wide Serine-Oriented Human Peptide Library. Biochemistry 2018, 57, 4717–4725. [PubMed: 29920078]

(20). Perez M; Blankenhorn J; Murray KJ; Parker LL High-throughput Identification of FLT3 Wild-type and Mutant Kinase Substrate Preferences and Application to Design of Sensitive In Vitro Kinase Assay Substrates. Mol. Cell. Proteomics 2019, 18, 477–489. [PubMed: 30541869]

(21). Choi J; Bomgarden R; Patel B; Foster L; Snovida S; Rogers J.c. Sequential Enrichment Using Metal Oxide Affinity Chromatography (SMOAC) to Enhance Phosphoproteome Coverage for Quantitative Proteomic Analysis; ThermoScientific, 2018.

(22). Suni V; Imanishi SY; Maiolica A; Aebersold R; Corthals GL Confident site localization using a simulated phosphopeptide spectral library. J. Proteome Res 2015, 14, 2348–2359. [PubMed: 25774671]

(23). Beausoleil SA; Villen J; Gerber SA; Rush J; Gygi SP A probability-based approach for high-throughput protein phosphorylation analysis and site localization. Nat. Biotechnol 2006, 24, 1285–1292. [PubMed: 16964243]

(24). Hulsen T; de Vlieg J; Alkema W. BioVenn - a web application for the comparison and visualization of biological lists using area-proportional Venn diagrams. BMC Genomics 2008, 9, No. 488.

(25). Mellacheruvu D; Wright Z; Couzens AL; Lambert JP; St-Denis NA; Li T; Miteva YV; Hauri S; Sardiu ME; Low TY; Halim VA; Bagshaw RD; Hubner NC; Al-Hakim A; Bouchard A; Faubert D; Fermin D; Dunham WH; Goudreault M; Lin ZY; Badillo BG; Pawson T; Durocher D; Coulombe B; Aebersold R; Superti-Furga G; Colinge J; Heck AJ; Choi H; Gstaiger M; Mohammed S; Cristea IM; Bennett KL; Washburn MP; Raught B; Ewing RM; Gingras AC; Nesvizhskii AI The CRAPome: a contaminant repository for affinity purification-mass spectrometry data. Nat. Methods 2013, 10, 730–736. [PubMed: 23921808]

(26). Saethang T; Hodge K; Yang CR; Zhao Y; Kimkong I; Knepper MA; Pisitkun T. PTM-Logo: a program for generation of sequence logos based on position-specific background amino-acid probabilities. Bioinformatics 2019, 35, 5313–5314. [PubMed: 31318409]

(27). Crooks GE; Hon G; Chandonia JM; Brenner SE WebLogo: a sequence logo generator. Genome Res. 2004, 14, 1188–1190. [PubMed: 15173120]

(28). Sugiyama N; Imamura H; Ishihama Y. Large-scale Discovery of Substrates of the Human Kinome. Sci. Rep 2019, 9, No. 10503.

(29). Rust HL; Thompson PR Kinase consensus sequences: a breeding ground for crosstalk. ACS Chem. Biol 2011, 6, 881–892. [PubMed: 21721511]

(30). Rawat S; Raman Suri C; Sahoo DK Molecular mechanism of polyethylene glycol mediated stabilization of protein. Biochem. Biophys. Res. Commun 2010, 392, 561–566. [PubMed: 20097167]

(31). Averill AM; Rehman HT; Charles JW; Dinh TA; Danyal K; Verschraegen CF; Stein GS; Dostmann WR; Ramsey JE Inhibition of the chimeric DnaJ-PKAc enzyme by endogenous inhibitor proteins. J. Cell. Biochem 2019, 120, 13783–13791. [PubMed: 30938854]

(32). Olivieri C; Walker C; Karamafrooz A; Wang Y; Manu VS; Porcelli F; Blumenthal DK; Thomas DD; Bernlohr DA; Simon SM; Taylor SS; Veglia G. Defective internal allosteric network imparts dysfunctional ATP/substrate-binding cooperativity in oncogenic chimera of protein kinase A. Commun. Biol. 2021, 4, No. 321.

(33). Badireddy S; Yunfeng G; Ritchie M; Akamine P; Wu J; Kim CW; Taylor SS; Qingsong L; Swaminathan K; Anand GS Cyclic AMP analog blocks kinase activation by stabilizing inactive conformation: conformational selection highlights a new concept in allosteric inhibitor design. Mol. Cell. Proteomics 2011, 10, No. M110004390.

(34). Dostmann WR (RP)-cAMPS inhibits the cAMP-dependent protein kinase by blocking the cAMP-induced conformational transition. FEBS Lett. 1995, 375, 231–234. [PubMed: 7498506]

(35). Wang Z; Cole PA Catalytic mechanisms and regulation of protein kinases. Methods Enzymol. 2014, 548, 1–21. [PubMed: 25399640]

(36). Zheng XL; Matsubara S; Diao C; Hollenberg MD; Wong NC Activation of apolipoprotein AI gene expression by protein kinase A and kinase C through transcription factor, Sp1. J. Biol. Chem 2000, 275, 31747–31754. [PubMed: 10829013]

(37). Farrow B; Rychahou P; Murillo C; O'Connor KL; Iwamura T; Evers BM Inhibition of pancreatic cancer cell growth and induction of apoptosis with novel therapies directed against protein kinase A. Surgery 2003, 134, 197–205. [PubMed: 12947318]

(38). Smith FD; Langeberg LK; Cellurale C; Pawson T; Morrison DK; Davis RJ; Scott JD AKAP-Lbc enhances cyclic AMP control of the ERK1/2 cascade. Nat. Cell Biol 2010, 12, 1242–1249. [PubMed: 21102438]

(39). Honda K. The biological role of actinin-4 (ACTN4) in malignant phenotypes of cancer. Cell Biosci. 2015, 5, No. 41.

(40). Bian Y; Song C; Cheng K; Dong M; Wang F; Huang J; Sun D; Wang L; Ye M; Zou H. An enzyme assisted RP-RPLC approach for in-depth analysis of human liver phosphoproteome. J. Proteomics 2014, 96, 253–262. [PubMed: 24275569]

(41). Carlson CR; Witczak O; Vossebein L; Labbe JC; Skalhegg BS; Keryer G; Herberg FW; Collas P; Tasken K. CDK1-mediated phosphorylation of the RIIalpha regulatory subunit of PKA works as a molecular switch that promotes dissociation of RIIalpha from centrosomes at mitosis. J. Cell Sci 2001, 114, 3243–3254. [PubMed: 11591813]

(42). Dephoure N; Zhou C; Villen J; Beausoleil SA; Bakalarski CE; Elledge SJ; Gygi SP A quantitative atlas of mitotic phosphorylation. Proc. Natl. Acad. Sci. U.S.A 2008, 105, 10762–10767. [PubMed: 18669648]

(43). Olsen JV; Vermeulen M; Santamaria A; Kumar C; Miller ML; Jensen LJ; Gnad F; CoX J; Jensen TS; Nigg EA; Brunak S; Mann M. Quantitative phosphoproteomics reveals widespread full phosphorylation site occupancy during mitosis. Sci. Signaling 2010, 3, No. ra3.

(44). Szklarczyk D; Gable AL; Lyon D; Junge A; Wyder S; Huerta-Cepas J; Simonovic M; Doncheva NT; Morris JH; Bork P; Jensen LJ; Mering CV STRING v11: protein-protein association networks with increased coverage, supporting functional discovery in genome-wide experimental datasets. Nucleic Acids Res. 2019, 47, D607–D613. [PubMed: 30476243]

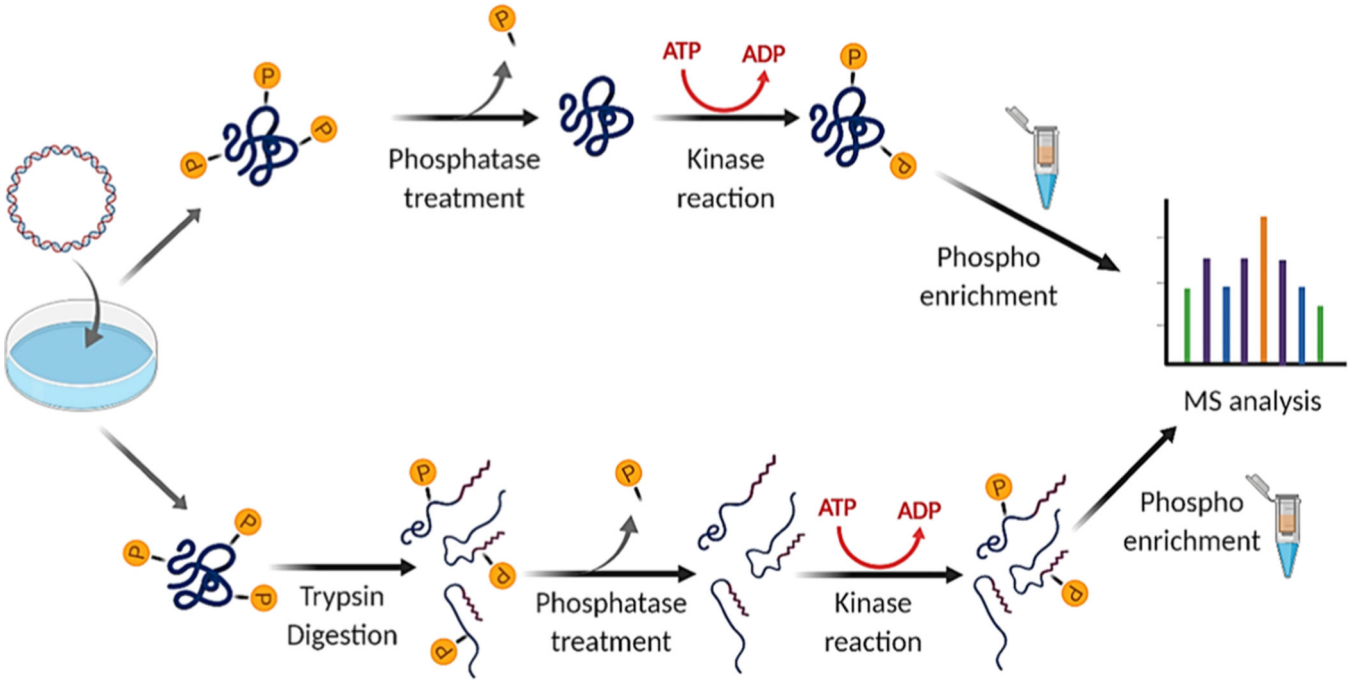

Figure 1.
Summary of workflow for protein-level (top) and peptide-level (bottom) KALIP rephosphorylation experiments (image created with BioRender).

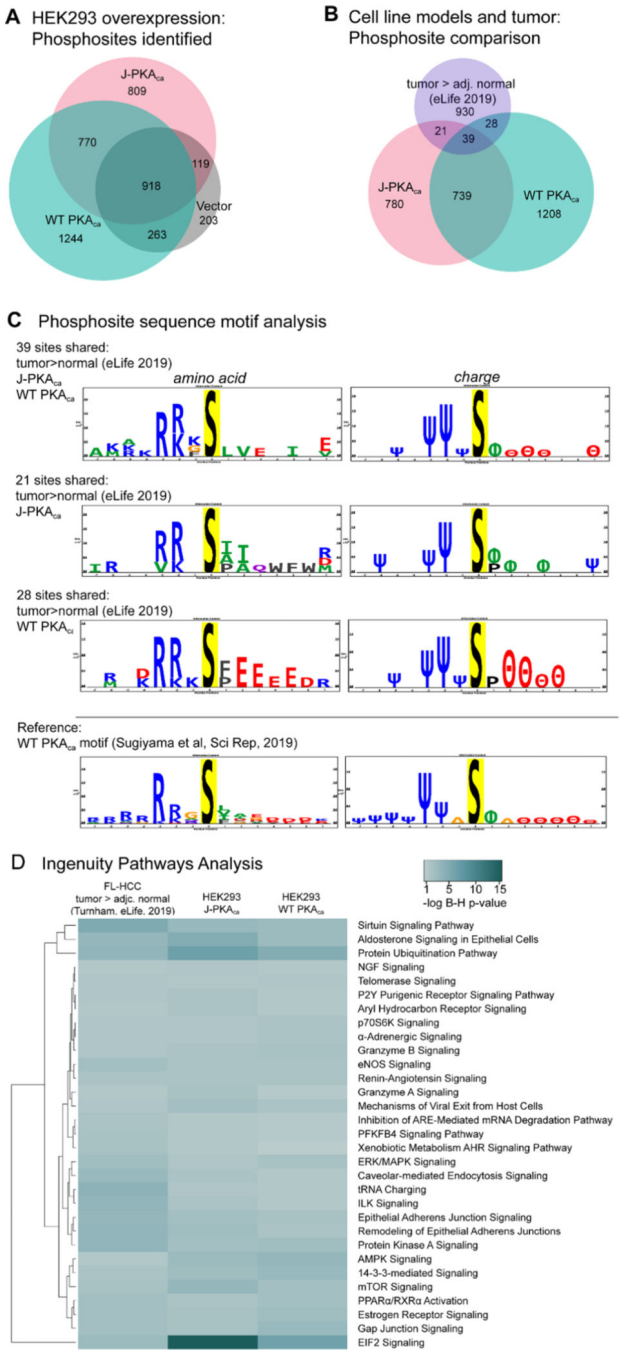

Figure 2.

Characteristics of phosphoprotein signaling and sites. (A) Venn diagram representing phosphosites confidently observed from PKA_{ca}- , J-PKA_{ca}-, and vector-only expressing cells (created using BioVenn https://www.biovenn.nl/). (B) Phosphosites observed (same lists used as input for IPA) were compared between the HEK293 overexpression models and FL-HCC tumor tissues (tumor > adj. normal, eLife, 2019[11]). Venn diagrams for comparisons of individual sites and for protein identifiers were created with BioVenn. (C) Sequence motif analysis for the overlapping phosphosite observations was performed using

PTM-Logo,[23] also including motif analysis for the sites observed as phosphorylated by WT PKA_{ca} in a previously reported study by Sugiyama et al. in 2019, performing whole-protein *in vitro* phosphorylation.[25] Only significantly over-represented amino acids and charge characteristics at positions −7 to +7 are shown in sequence logos. Charge logo legend: Ψ = basic residue, e.g., K/R; θ = acidic residue, e.g., D/E; ϕ = hydrophobic residue; P = proline; Δ = other. (D) Heatmap generated with https://heatmapper.ca, illustrating selected pathway activation enrichment scores from IPA (Supporting Table S3), comparing phosphorylation sites observed as higher in tumor *vs* normal FL-HCC tissue in the Turnham et al. study *vs* HEK293 cells overexpressing J-PKA_{ca} or WT PKA_{ca} (after filtering each to remove sites observed in vector-only control). Multiple comparison-corrected Benjamini–Hochberg p-values were determined in IPA, with the significance cutoff set at p = 0.05, and only pathways with significant B–H p-value enrichment scores from the Turnham data and the J-PKA_{ca} data were included in the heatmap.

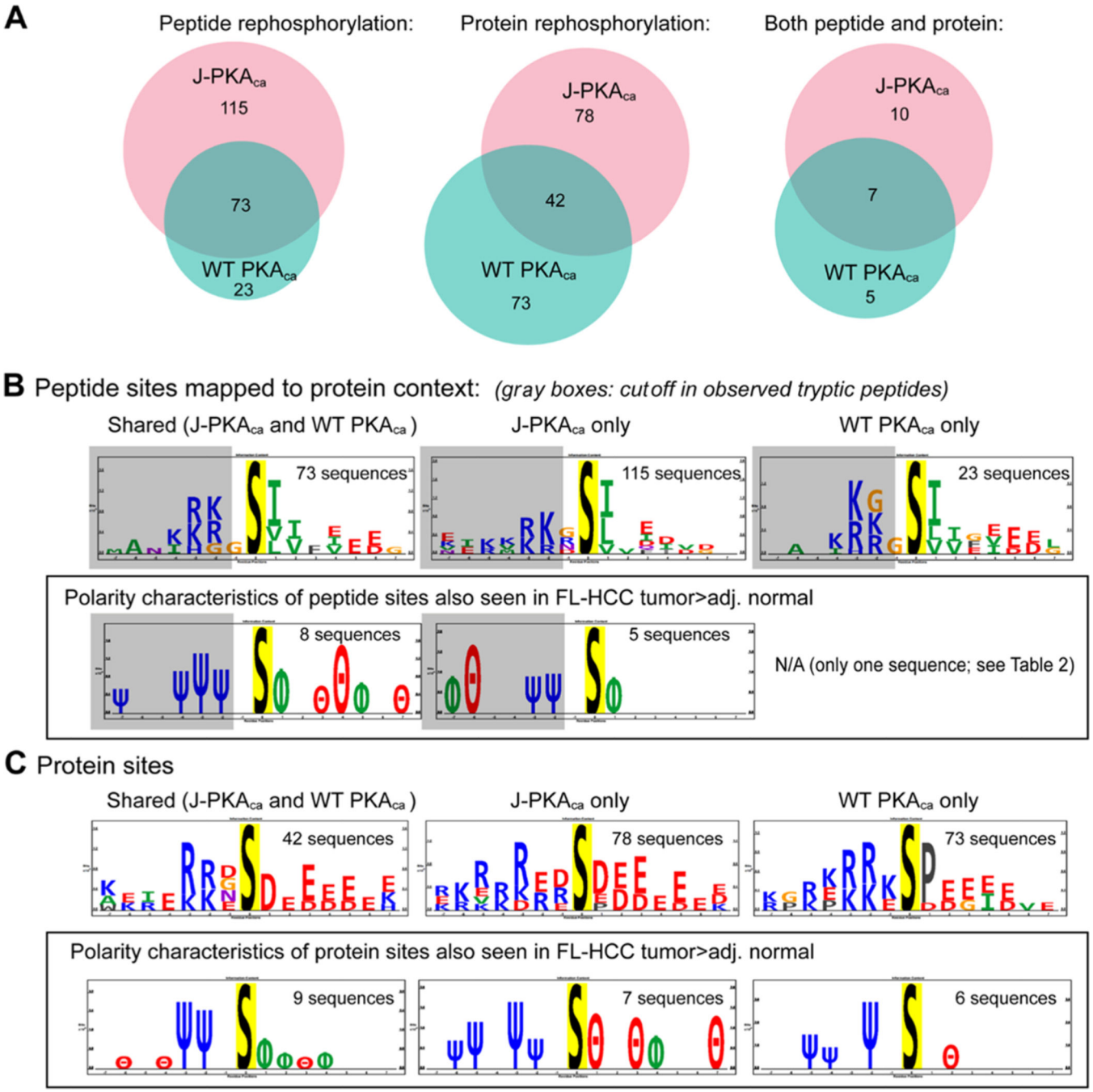

Figure 3.

Peptide and protein rephosphorylation experiments. (A) Venn diagrams illustrating the number of phosphopeptides robustly observed in both replicates of the peptide and/or protein rephosphorylation experiment using recombinant J-PKA$_{ca}$ or WT PKA$_{ca}$, showing common and unique peptides for each. (B) Sequence motif analysis using PTM-logo[23] (sites mapped to their protein context) for peptide rephosphorylation experiment, overall (top) and highlighting amino acid polarity characteristics for those also seen as higher in FL-HCC tumors by Turnham et al.[11] (in a box). Almost all observed phosphopeptides were

truncated within 1–2 amino acid N-terminals of the phosphosite (illustrated by gray boxes in sequence logos). Number of sequences used to generate motifs provided for context. (C) Sequence motifs for sites observed by protein rephosphorylation, including all sites observed (top; likely contains upstream/downstream sites as well as direct) and those also seen as more abundant in FL-HCC tumor tissues[11] (as for peptide rephosphorylation in a box). Additional detailed information (UniProt identifiers, phosphosites, tc.) provided in Table 2 and Supporting Table S1. Charge logo legend: Ψ = basic residue, e.g., K/R; θ = acidic residue, e.g., D/E; ϕ = hydrophobic residue; P = proline; Δ = other.

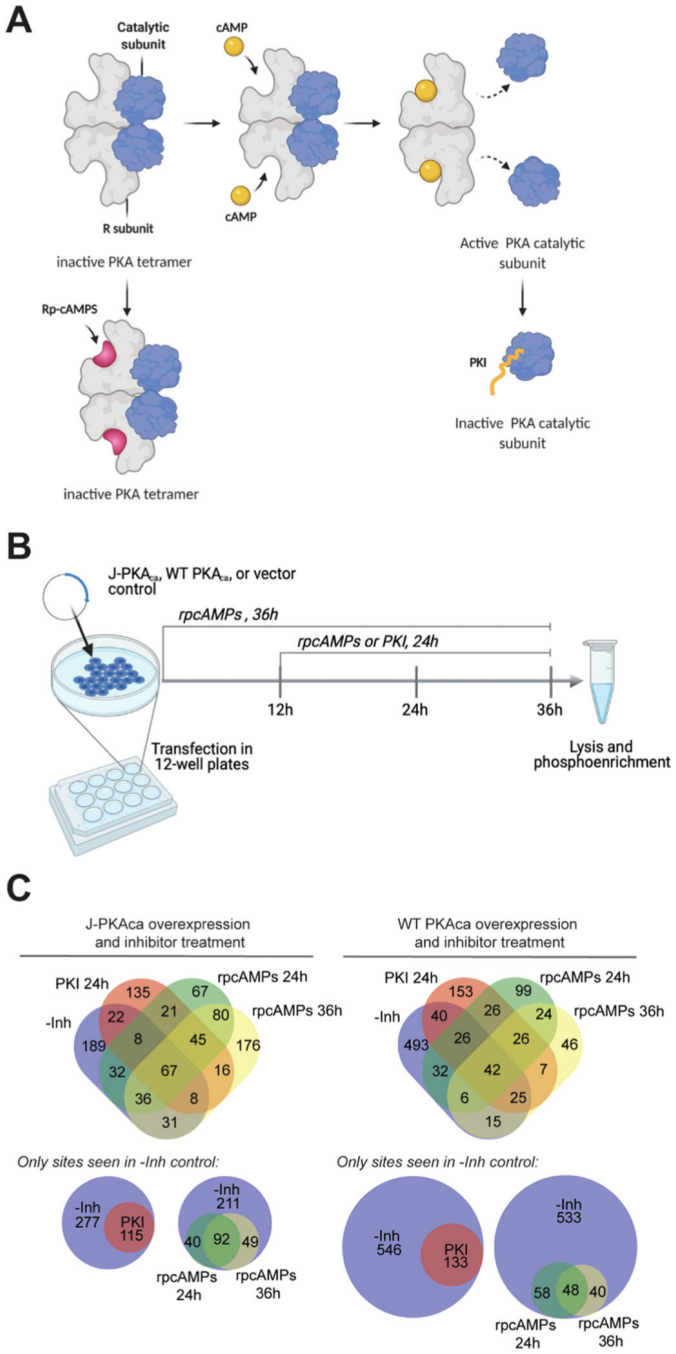

Figure 4.

Phosphoproteomics of inhibitor-treated cells. (A) Different mechanisms of inhibition for two cAMP-PKA specific inhibitors PKI and rpcAMPs. rpcAMP binds to the PKA regulatory subunit and prevents its dissociation from the catalytic subunit and is also resistant toward cyclic nucleotide phosphodiesterases. PKI is a substrate-competitive inhibitor of the catalytic subunit. (B) Experimental design: cells cultured in 12-well plates were transfected in duplicate with J-PKA_{ca}, WT PKA_{ca}, or empty vector and incubated for 36 h. Inhibitor was added at $t = 0$ h (rpcAMPs) or $t = 12$ h (PKI or rpcAMPs) for 36 or 24 h

treatment, followed by lysis, trypsin digest, and phosphoenrichment for LC-MS/MS (created with BioRender.com). (C) Venn diagrams illustrating the outcomes from experiments by kinase construct and inhibitor. Top: four-way Venn diagrams (created with http://bioinformatics.psb.ugent.be/webtools/Venn/) showing numbers of phosphosites identified in each sample but not the corresponding vector-only control. Bottom: subsetted, simplified proportional Venn diagrams (created with http://biovenn.nl) showing only phosphosites observed in the -Inh controls and the various inhibitor treatments.

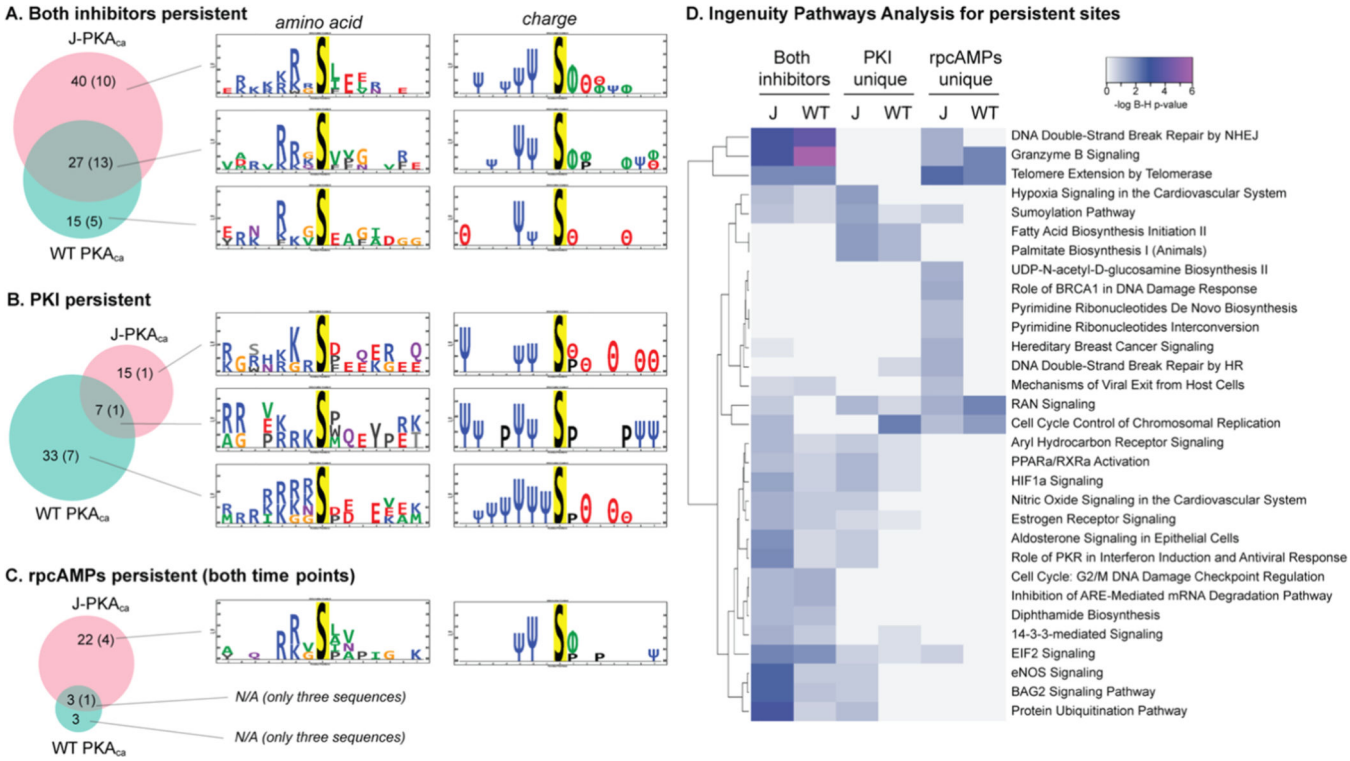

Figure 5.

Motifs observed for persistent phosphosites. Venn diagrams for number of sites that persisted in the presence of inhibitors for each kinase construct (number of those that also had evidence that they may be direct substrates indicated in parentheses) and amino acid/polarity motifs for the sets of sequences associated with each group. (A) Both inhibitors, all time points. (B) Persisting through PKI but not rpcAMPs. (C) Persisting through both time courses of rpcAMPs but not PKI (Venn diagrams created with http://biovenn.nl; motif logos created with PTM-logo[23]). Charge logo legend: Ψ = basic residue, e.g., K/R; θ = acidic residue, e.g., D/E; ϕ = hydrophobic residue; P = proline. (D) Heatmap generated using https://heatmapper.ca illustrating ingenuity pathways analysis (Supporting Table S4) showing the $\log_{10}$ Benjamini–Hochberg p-values for enrichment of canonical pathways represented by the sites observed as persistent in the presence of both inhibitors or uniquely for each inhibitor, per kinase construct. J = K-PKA$_{ca}$; WT = WT PKA$_{ca}$.

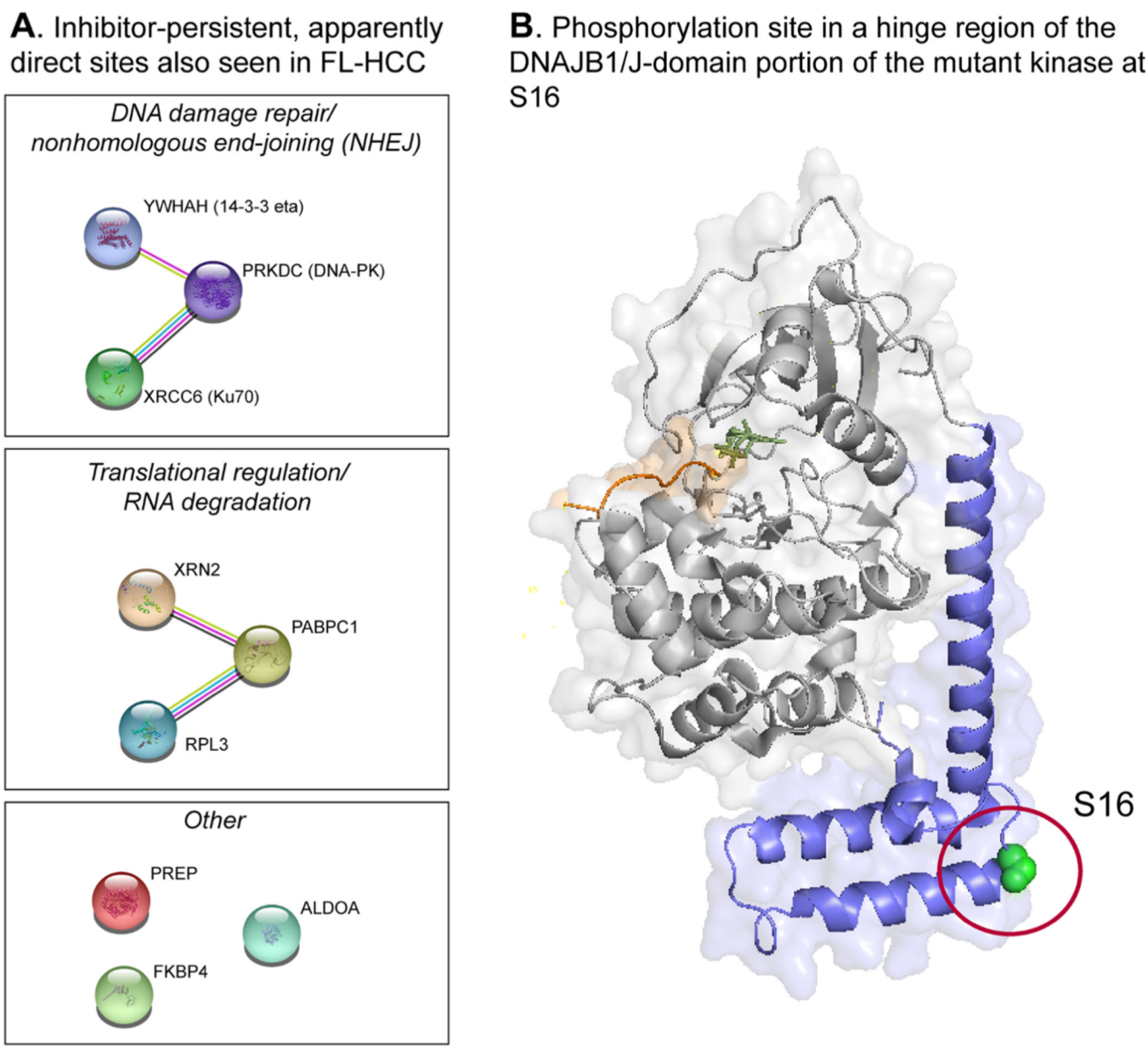

Figure 6. Specific sites of interest.

(A) Potential functional relationships between the proteins with sites we observed in direct phosphorylation experiments that were also seen in FL-HCC by Turnham et al.[10] and to persist across conditions in our inhibitor experiments (J-PKA$_{ca}$ and WT PKA$_{ca}$). (B) Illustration showing the location of the phosphosite observed for the J-domain (adapted from PDB entry 4WB7).

Table 1.

Comparing Sites Observed in FL-HCC Tissue (Higher in Tumor *vs* Adjacent Normal; Turnham et al., eLife, 2019)[11] and the HEK293 J-PKA_{ca} and/or WT PKA_{ca} Overexpression Models

						all three
uniprot ID	**gene name**	**entry name**	**protein name**	**site**	**sequence**	**direct**[a]
P12956	XRCC6	XRCC6_HUMAN	X-ray repair cross-complementing protein 6 (Ku70)	520	AMNKRLGSLVDEFKE	xxxx
P39023	RPL3	RL3_HUMAN	60S ribosomal protein L3	13	FSAPRHGSLGFLPRK	xxxx
Q02790	FKBP4	FKBP4_HUMAN	peptidyl-prolyl cis-trans isomerase FKBP4	78	LDRKDKFSFDLGKGE	xx
Q08211	DHX9	DHX9_HUMAN	ATP-dependent RNA helicase A (DEAH box protein 9)	449	VTQPRRISAVSVAER	xx
Q04917	YWHAH	1433F_HUMAN	14–3-3 protein eta (protein AS1)	145	ASGEKKNSVVEASEA	xx
Q14690	PDCD11	RRP5_HUMAN	protein RRP5 homologue (NF-kappa-B-binding protein)	926	ARKLRKGSEHQAIVQ	x
P11940	PABPC1	PABP1_HUMAN	polyadenylate-binding protein 1 (PABP-1)	96	RDPSLRKSGVGNIFI	x
P48147	PREP	PPCE_HUMAN	prolyl endopeptidase (PE)	667	VGRSRKQSNPLLIHV	x
P62888	RPL30	RL30_HUMAN	60S ribosomal protein L30	10	AAKKTKKSLESINSR	x
Q9Y2W1	THRAP3	TR150_HUMAN	thyroid hormone receptor-associated protein 3	377	EKIKEKGSFSDTGLG	x
Q9H0D6	XRN2	XRN2_HUMAN	5′– 3′ exoribonuclease 2	678	PEETRRNSLGGDVLF	x
P14625	HSP90B1	ENPL_HUMAN	endoplasmin (94 kDa glucose-regulated protein) (GRP-94)	306	AKEEKEESDDEAAVE	x
P48444	ARCN1	C0PD_HUMAN	coatomer subunit delta (delta-coat protein)	437	RHDSRRNTLEWCLPV	
Q5T5Y3	CAMSAP1	CAMP1_HUMAN	calmodulin-regulated spectrin-associated protein 1	629	SIVSRRPSEGPQPLV	
060716	CTNND1	CTND1_HUMAN	catenin delta-1 (cadherin-associated Src substrate)	268	PQVRVGGSSVDLHRF	
P12081	HARS1	HARS1_HUMAN	histidine-tRNA ligase, cytoplasmic	27	GLKQQKASAELIEEE	
P08670	VIM	VIME_HUMAN	vimentin	72	SSAVRLRSSVPGVRL	
Q8WUI4	HDAC7	HDAC7_HUMAN	histone deacetylase 7	573	CLRGRKASLEELQSV	
Q6P2E9	EDC4	EDC4_HUMAN	enhancer of mRNA-decapping protein 4	1389	GKAARRLSLMLHGLV	
P53618	C0PB1	C0PB_HUMAN	coatomer subunit β (β-coat protein)	933	HIRIRAKSQGMALSL	
095757	HSPA4L	HS74L_HUMAN	heat shock 70 kDa protein 4L	579	LKKGKVKSIDLPIQS	
Q15149	PLEC	PLEC_HUMAN	plectin	2886	PVRNRRLTVNEAVKE	
Q09666	AHNAK	AHNK_HUMAN	neuroblast differentiation-associated protein AHNAK	332	PKAGLRVSAPEVSVG	
000560	SDCBP	SDCB1_HUMAN	syntenin-1	131	KIGLRLKSIDNGIFV	
Q13501	SQSTM1	SQSTM_HUMAN	sequestosome-1	272	RSRLTPVSPESSSTE	

all three

uniprot ID	gene name	entry name	protein name	site	sequence	direct[a]
Q15149	PLEC	PLEC_HUMAN	plectin	3785	DYVRRRLTAEDLFEA	
P22626	HNRNPA2B1	R0A2_HUMAN	heterogeneous nuclear ribonucleoproteins A2/B1	225	NFGPGPGSNFRGGSD	
P11586	MTHFD1	C1TC_HUMAN	C1-tetrahydrofolate synthase, cytoplasmic (C1-THF synthase)	490	VNGVRRFSDIQIRRL	
Q7Z406	MYH14	MYH14_HUMAN	myosin-14 (myosin heavy chain 14)	105	RMNPPKFSKAEDMAE	
095613	PCNT	PCNT_HUMAN	pericentrin	1814	ADQERRHSQALEALQ	
P35579	MYH9	MYH9_HUMAN	myosin-9	81	KMNPPKFSKVEDMAE	
Q14980	NUMA1	NUMA1_HUMAN	nuclear mitotic apparatus protein 1	2047	KQADRRQSMAFSILN	
P27816	MAP-4	MAP4_HUMAN	microtubule-associated protein 4 (MAP-4)	636	TGTGKKCSLPAEEDS	
P13861	PRKAR2A	KAP2_HUMAN	cAMP-dependent protein kinase type II-α regulatory subunit	58	PAATPRQSLGHPPPE	
P98174	FGD1	FGD1_HUMAN	FYVE, RhoGEF, and PH domain-containing protein 1	135	EGPQRLRSDPGPPTE	
P47897	QARS1	SYQ_HUMAN	glutamine-tRNA ligase	70	LRDTRRLSFLVSYIA	
Q8NDT2	RBM15B	RB15B_HUMAN	putative RNA-binding protein 15B	532	ADLVRDRTPPHLLYS	
095140	MFN2	MFN2_HUMAN	mitofusin-2	442	AEEIRRLSVLVDDYQ	
060832	DKC1	DKC1_HUMAN	H/ACA ribonucleoprotein complex subunit DKC1	21	KKKKERKSLPEEDVA	

J-PKAca cells and FL-HCC

uniprot ID	gene name	entry name	protein name	site	sequence	direct[a]
043707	ACTN4	ACTN4_HUMAN	α-actinin-4 (nonmuscle α-actinin-4)	423	EKFRQKASIHEAWTD	xxx
014579	C0PE	C0PE_HUMAN	coatomer subunit epsilon	99	AHESRRDSIVAELDR	xx
P10809	HSPD1	CH60_HUMAN	60 kDa heat shock protein, mitochondrial (Hsp60)	488	KNAGVEGSLIVEKIM	xx
Q14204	DYNC1H1	DYHC1_HUMAN	cytoplasmic dynein 1 heavy chain 1	1230	DIMRRKDSAIQQQVA	xx
P07900	HSP90AA1	HS90A_HUMAN	heat shock protein HSP 90-α	641	LEINPDHSIIETLRQ	x
P21333	FLN-A	FLNA_HUMAN	filamin-A (FLN-A)	1084	LQGGSAGSPARFTID	
Q16637	SMN1	SMN_HUMAN	survival motor neuron protein (Gemin-1)	28	FRRGTGQSDDSDIWD	
P61604	HSPE1	CH10_HUMAN	10 kDa heat shock protein, mitochondrial (Hsp10)	21	DRVLVERSAAETVTK	
060825	PFKFB2	F262_HUMAN	6-phosphofructo-2-kinase/fructose-2,6-bisphosphatase 2	466	PVRMRRNSFTPLSSS	
Q12955	ANK3	ANK3_HUMAN	ankyrin-3	1459	EKTDRRQSFASLALR	
P02545	LMNA	LMNA_HUMAN	prelamin-A/C [cleaved into: lamin-A/C (70 kDa lamin)]	392	ERLRLSPSPTSQRSR	
Q9UI14	RABAC1	PRAF1_HUMAN	prenylated Rab acceptor protein 1	41	WLERRRATIRPWSTF	
Q08211	DHX9	DHX9_HUMAN	ATP-dependent RNA helicase A	1142	IRQISRPSAAGINLM	

J Proteome Res. Author manuscript; available in PMC 2023 May 02.

all three

uniprot ID	gene name	entry name	protein name	site	sequence	direct[a]
P83731	RPL24	RL24_HUMAN	60S ribosomal protein L24	149	IVKPVKVSAPRVGGK	
Q15126	PMVK	PMVK_HUMAN	phosphomevalonate kinase (PMKase)	113	VSDTRRVSDIQWFRE	

J-PKAca cells and FL-HCC

uniprot ID	gene name	entry name	protein name	site	sequence	direct[a]
Q9NZU5	LMCD1	LMCD1_HUMAN	LIM and cysteine-rich domains protein 1	16	NPGVKKMSLGQLQSA	
Q8IVT5	KSR1	KSR1_HUMAN	kinase suppressor of Ras 1	888	PKLNRRLSHPGHFWK	
043707	ACTN4	ACTN4_HUMAN	α-actinin-4 (nonmuscle α-actinin-4)	367	LQTKLRLSNRPAFMP	
Q14789	G0LGB1	G0GB1_HUMAN	golgin subfamily B member 1	2489	QLEERHLSIILEKDQ	
Q06210	GFPT1	GFPT1_HUMAN	glutamine-fructose-6-phosphate aminotransferase 1	205	AVGTRRGSPLLIGVR	
060488	ACSL4	ACSL4_HUMAN	long-chain-fatty-acid-CoA ligase 4	674	IPIKVRLSPEPWTPE	

WT PKAca cells and FL-HCC

uniprot ID	gene name	entry name	protein name	site	sequence	direct[a]
P11142	HSPA8	HSP7C_HUMAN	heat shock cognate 71 kDa protein	329	RDAKLDKSQIHDIVL	xx
P11142	HSPA8	HSP7C_HUMAN	heat shock cognate 71 kDa protein	511	TNDKGRLSKEDIERM	x
P78559	MAP-1A	MAP1A_HUMAN	microtubule-associated protein 1A (MAP-1A)	667	EMEEVHPSDEEEEDA	
P17096	HMGA1	HMGA1_HUMAN	high mobility group protein HMG-I/HMG-Y	102	EEGISQESSEEEQ__	
Q8NDT2	RBM15B	RB15B_HUMAN	putative RNA-binding protein 15B	609	DRGRTTHSPYEERSR	
Q8WWI1	LM0–7	LM07_HUMAN	LIM domain only protein 7 (LMO-7)	246	RHHKREDSFESLDSL	
P27708	CAD	PYR1_HUMAN	CAD protein (pyrimidine biosynthesis fusion complex)	1406	GAGGRRLSSFVTKGY	
Q16643	DBN1	DREB_HUMAN	drebrin	142	NGLARLSSPVLHRLR	
P49736	MCM2	MCM2_HUMAN	DNA replication licensing factor MCM2	139	RRGLLYDSDEEDEER	
Q00610	CLTC	CLH1_HUMAN	clathrin heavy chain 1	191	YSVDRKVSQPIEGHA	
Q9NZB2	FAM120A	F120A_HUMAN	constitutive coactivator of PPAR-γ-like protein 1	30	LQKLARGSLVGGGRQ	
Q96S38	RPS6KC1	KS6C1_HUMAN	ribosomal protein S6 kinase delta-1 (S6K-delta-1)	427	LNRSPEESFDIKEVK	
Q9NNW5	WDR6	WDR6_HUMAN	WD repeat-containing protein 6	514	VCGDRRGSVLLFPSR	
P02545	LMNA	LMNA_HUMAN	prelamin-A/C [cleaved into: lamin-A/C (70 kDa lamin)]	51	VYIDRVRSLETENAG	
Q9UK76	JPT1	JUPI1_HUMAN	Jupiter microtubule-associated homologue 1	87	SGLQRRNSSEASSGD	
Q8WX93	PALLD	PALLD_HUMAN	palladin	1121	PRSRSRDSGDENEPI	

J Proteome Res. Author manuscript; available in PMC 2023 May 02.

all three

uniprot ID	gene name	entry name	protein name	site	sequence	direct[a]
P46821	MAP-1B	MAP1B_HUMAN	microtubule-associated protein 1B (MAP-1B)	832	AERSLMSSPEDLTKD	
Q5JRA6	MIA3	TG01_HUMAN	transport and Golgi organization protein 1 homologue (TANGO1)	1539	MALQKKLSQEEYERQ	
Q92905	C0PS5	CSN5_HUMAN	COP9 signalosome complex subunit 5	284	EAQLGRGSFMLGLET	
Q02952	AKAP12	AKA12_HUMAN	A-kinase anchor protein 12 (AKAP12)	627	KKRVRRPSESDKEDE	
P21359	NF-1	NF1_HUMAN	neurofibromin (neurofibromatosis-related protein NF-1)	2543	KLLGTRKSFDHLISD	
Q9C0C9	UBE20	UBE20_HUMAN	(E3-independent) E2 ubiquitin-conjugating enzyme	515	SGTSRKKSIPLSIKN	
Q96S38	RPS6KC1	KS6C1_HUMAN	ribosomal protein S6 kinase delta-1 (S6K-delta-1)	423	ISKFLNRSPEESFDI	
Q6UX71	PLXDC2	PXDC2_HUMAN	plexin domain-containing protein 2	506	AMKFRRGSGHPAYAE	
Q86UU1	PHLDB1	PHLB1_HUMAN	pleckstrin homology-like domain family B member 1	324	GGHERPPSPGLRGLL	
094806	PRKD3	KPCD3_HUMAN	serine/threonine-protein kinase D3 (protein kinase C nutype)	731	ARIIGEKSFRRSVVG	
A6NHR9	SMCHD1	SMHD1_HUMAN	structural maintenance of chromosomes flexible hinge domain-containing protein 1	1697	ALLKRKLSEQEELKK	
Q15084	PDIA6	PDIA6_HUMAN	protein disulfide-isomerase A6	428	VEDDIDLSDVELDDL	

[a]Number of direct phosphorylation observations at the protein or peptide level (see Supporting Table S1).

Table 2.

Summary of Phosphosites Seen in FL-HCC Tumor > Adj. Normal (Turnham)[11] and as Direct Substrates in Rephosphorylation Reactions by J-PKA$_{ca}$ and/or WT PKA$_{ca}$ *In Vitro*

all three

uniprot ID	gene name	entry name	protein name	site	sequence	peptide	protein
P12956	XRCC6	XRCC6_HUMAN	X-ray repair cross-complementing protein 6 (Ku70)	520	AMNKRLGSLVDEFKE	x	x
P39023	RPL3	RL3_HUMAN	60S ribosomal protein L3	13	FSAPRHGSLGFLPRK	x	x
P60174	TPI1	TPIS_HUMAN	triosephosphate isomerase	21	KMNGRKQSLGELIGT	x	x
043707	ACTN4	ACTN4_HUMAN	α-actinin-4	423	EKFRQKASIHEAWTD	x	x[a]
Q02790	FKBP4	FKBP4_HUMAN	peptidyl-prolyl cis-trans isomerase FKBP4	78	LDRKDKFSFDLGKGE	x[a]	x[a]
014579	COPE	C0PE_HUMAN	coatomer subunit epsilon	99	AHESRRDSIVAELDR	x	
P10809	HSPD1	CH60_HUMAN	60 kDa heat shock protein, mitochondrial	488	KNAGVEGSLIVEKIM	x	
P11142	HSPA8	HSP7C_HUMAN	heat shock cognate 71 kDa protein	329	RDAKLDKSQIHDIVL	x	
P04075	ALDOA	ALD0A_HUMAN	fructose-bisphosphate aldolase A	46	SIAKRLQSIGTENTE	x	
Q08211	DHX9	DHX9_HUMAN	ATP-dependent RNA helicase A	449	VTQPRRISAVSVAER		x
Q04917	YWHAH	1433F_HUMAN	14–3-3 protein eta	145	ASGEKKNSVVEASEA		x
Q14204	DYNC1H1	DYHC1_HUMAN	cytoplasmic dynein 1 heavy chain 1	1230	DIMRRKDSAIQQQVA		x
095819	MAP4K4	M4K4_HUMAN	mitogen-activated protein kinase kinase kinase kinase 4	900	QDPTRKGSVVNVNPT		x
P16949	STMN1	STMN1_HUMAN	stathmin	16	KELEKRASGQAFELI		x
P78527	PRKDC	PRKDC_HUMAN	DNA-dependent protein kinase catalytic subunit	893	WDREKRLSFAVPFRE		x

J-PKAca rephosphorylation and FL-HCC

uniprot ID	gene name	entry name	protein name	site	sequence	peptide	protein
Q9Y2W1	THRAP3	TR150_HUMAN	thyroid hormone receptor-associated protein 3	377	EKIKEKGSFSDTGLG	x	
Q9H0D6	XRN2	XRN2_HUMAN	5′–3′ exoribonuclease 2 (DHM1-like protein)	678	PEETRRNSLGGDVLF	x	
P07900	HSP90AA1	HS90A_HUMAN	heat shock protein HSP 90-α	641	LEINPDHSIIETLRQ	x	
P62987	UBA52	RL40_HUMAN	ubiquitin-60S ribosomal protein L40	57	LEDGRTLSDYNIQKE	x	
P31040	SDHA	SDHA_HUMAN	succinate dehydrogenase flavoprotein subunit, mitochondrial	530	AAVFRVGSVLQEGCG	x	
P14625	HSP90B1	ENPL_HUMAN	endoplasmin (94 kDa glucose-regulated protein)	306	AKEEKEESDDEAAVE		x
060749	SNX2	SNX2_HUMAN	sorting nexin-2	185	FSVKRRFSDFLGLHS		x
P49419	ALDH7A1	AL7A1_HUMAN	α-aminoadipic semialdehyde dehydrogenase	84	IARVRQASVADYEET		x

all three

uniprot ID	gene name	entry name	protein name	site	sequence	peptide	protein
Q9Y230	RUVBL2	RUVB2_HUMAN	RuvB-like 2	419	VCRKRKGTEVQVDDI		x
Q9NR30	DDX21	DDX21_HUMAN	nucleolar RNA helicase 2	121	VTKNEEPSEEEIDAP		x
Q02543	RPL18A	RL18A_HUMAN	60S ribosomal protein L18a	123	RHRARAHSIQIMKVE		x
P27708	CAD	PYR1_HUMAN	CAD protein (pyrimidine biosynthesis fusion complex)	1859	PPRIHRASDPGLPAE		x

WT PKAca rephosphorylation and FL-HCC

uniprot ID	gene name	entry name	protein name	site	sequence	peptide	protein
P34932	HSPA4	HSP74_HUMAN	heat shock 70 kDa protein 4	76	RFHGRAFSDPFVEAE	x	
Q14690	PDCD11	RRP5_HUMAN	protein RRP5 homologue (programmed cell death protein 11)	926	ARKLRKGSEHQAIVQ		x
P11940	PABPC1	PABP1_HUMAN	polyadenylate-binding protein 1	96	RDPSLRKSGVGNIFI		x
P48147	PREP	PPCE_HUMAN	prolyl endopeptidase	667	VGRSRKQSNPLLIHV		x
P62888	RPL30	RL30_HUMAN	60S ribosomal protein L30	10	AAKKTKKSLESINSR		x
P11142	HSPA8	HSP7C_HUMAN	heat shock cognate 71 kDa protein	511	TNDKGRLSKEDIERM		x

[a] Seen in either J-PKA_{ca} or WT PKA_{ca} rephosphorylation but not both; see Supporting Table S1 for details.

J Proteome Res. Author manuscript; available in PMC 2023 May 02.

Table 3.

Persistent Phosphorylation Sites Observed

persistently observed: both kinase constructs, each inhibitor, all time points

uniprot ID	gene name	entry name	protein name	site	sequence	in Turnham tumor > normal?	direct evidence?
P08670	VIM	VIME_HUMAN	vimentin	72	SSAVRLRSSVPGVRL	x	
P11940	PABPCi	PABP1_HUMAN	polyadenylate-binding protein 1 (PABP-1)	96	RDPSLRKSGVGNIFI	x	x
P12956	XRCC6	XRCC6_HUMAN	X-ray repair cross-complementing protein 6 (Ku70)	520	AMNKRLGSLVDEFKE	x	xxxx
P13861	PRKAR2A	KAP2_HUMAN	cAMP-dependent protein kinase type II-α regulatory subunit	58	PAATPRQSLGHPPPE	x	
P48147	PREP	PPCE_HUMAN	prolyl endopeptidase	667	VGRSRKQSNPLLIHV	x	x
Q02790	FKBP4	FKBP4_HUMAN	peptidyl-prolyl cis—trans isomerase FKBP4	78	LDRKDKFSFDLGKGE	x	xx
Q04917	YWHAH	1433F_HUMAN	14–3-3 protein eta	145	ASGEKKNSVVEASEA	x	xx
P78527	PRKDC	PRKDC_HUMAN	DNA-dependent protein kinase catalytic subunit	893	WDREKRLSFAVPFRE	x	xx
P55010	EIF5	IF5_HUMAN	eukaryotic translation initiation factor 5	410	VVYSKAASVPKVETV		
O00231	PSMD11	PSD11_HUMAN	26S proteasome non-ATPase regulatory subunit 11	14	VEFQRAQSLLSTDRE		x
P26373	RPL13	RL13_HUMAN	60S ribosomal protein L13	77	VRAGRGFSLEELRVA		x
P08670	VIM	VIME_HUMAN	vimentin	73	SAVRLRSSVPGVRLL		
Q9P2K5	MYEF2	MYEF2_HUMAN	myelin expression factor 2 (MEF-2)	520	GMRERIGSKGNQIFV		
P52272	HNRNPM	HNRPM_HUMAN	heterogeneous nuclear ribonucleoprotein M	365	ENMGRFGSGMNMGRI	-	
P23588	EIF4B	IF4B_HUMAN	eukaryotic translation initiation factor 4B (eIF-4B)	359	SQSTRAASIFGGAKP		
Q12872	SFSWAP	SFSWA_HUMAN	splicing factor, suppressor of white-apricot homologue	238	KAKQARNSQFDFLRF		
Q14980	NUMA1	NUMA1_HUMAN	nuclear mitotic apparatus protein 1	1969	QETLRRASMQPIQIA		
Q9NR30	DDX21	DDX21_HUMAN	nucleolar RNA helicase 2	487	LKGFRNGSFGVLVAT		
P52272	HNRNPM	HNRPM_HUMAN	heterogeneous nuclear ribonucleoprotein M	397	GGGGGGGSVPGIERM		x
Q13310	PABPC4	PABP4_HUMAN	polyadenylate-binding protein 4 (PABP-4)	96	RDPSLRKSGVGNVFI		
P07900	HSP90AAi	HS90A_HUMAN	heat shock protein HSP 90-α	330	HLAVKHFSVEGQLEF		xx
Q9UHXi	PUF60	PUF60_HUMAN	poly(U)-binding-splicing factor PUF60	206	NIKVGRPSNIGQAQP		x
Q14320	FAM50A	FA50A_HUMAN	protein FAM50A	276	VTKARGKSGPLFNFD		x
Q6P2Q9	PRPF8	PRP8_HUMAN	pre-mRNA-processing-splicing factor 8	2079	EWRVRAISAANLHLR		
P50502	ST13	F10A1_HUMAN	Hsc70-interacting protein (Hip)	156	ILYAKRASVFVKLQK		
P20700	LMNBi	LMNBi_HUMAN	lamin-B1	158	TALGDKKSLEGDLED		

persistently observed: both kinase constructs, each inhibitor, all time points

uniprot ID	gene name	entry name	protein name	site	sequence	in Turnham tumor > normal?	direct evidence?
P13639	EEF2	EF2_HUMAN	elongation factor 2 (EF-2)	23	KANIRNMSVIAHVDH		xx